INVESTIGATION OF PRESSURE SURGES DUE TO VALVE ACTIONS IN WELLBORES TO ESTIMATE RESERVOIR PARAMETERS

A THESIS SUBMITTED TO
THE GRADUATE SCHOOL OF NATURAL AND APPLIED SCIENCES
OF
MIDDLE EAST TECHNICAL UNIVERSITY

BY

TABİAT TAN YILDIZ

IN PARTIAL FULFILLMENT OF THE REQUIREMENTS
FOR
THE DEGREE OF DOCTOR OF PHILOSOPHY
IN
PETROLEUM AND NATURAL GAS ENGINEERING

July 2025

Approval of the Thesis:

INVESTIGATIONS OF PRESSURE SURGES DUE TO VALVE ACTIONS IN WELLBOORES TO ESTIMATE RESERVOIR PARAMETERS

submitted by **TABİAT TAN YILDIZ** in partial fulfillment of the requirements for the degree of **Doctor of Philosophy** i**n Petroleum and Natural Gas Engineering, Middle East Technical University** by,

Prof. Dr. Naci Emre Altun
Dean, **Graduate School of Natural and Applied Sciences** _____

Assoc. Prof. Dr. İsmail Durgut
Head of the Department, **Petroleum and Natural Gas Eng** _____

Assoc. Prof. Dr. İsmail Durgut
Supervisor, **Petroleum and Natural Gas Eng, METU** _____

Examining Committee Members:

Assoc. Prof. Dr. Çağlar Sınayuç
Petroleum and Natural Gas Engineering Dept., METU _____

Assoc. Prof. Dr. İsmail Durgut
Petroleum and Natural Gas Engineering Dept., METU _____

Prof. Dr. Murat Uysal
Electrical and Electronics Eng. Dept., Özyeğin University _____

Asst. Prof. Dr. Gamze İpek
Petroleum and Natural Gas Engineering Dept., METU NCC _____

Asst. Prof. Dr. Mehmet Onur Doğan
Petroleum and Natural Gas Engineering Dept., METU _____

Date: 09.07.2025

I hereby declare that all information in this document has been obtained and presented in accordance with academic rules and ethical conduct. I also declare that, as required by these rules and conduct, I have fully cited and referenced all material and results that are not original to this work.

Name Last name : Tabiat Tan Yıldız
Signature :

ABSTRACT

INVESTIGATION OF PRESSURE SURGES DUE TO VALVE ACTIONS IN WELLBORES TO ESTIMATE RESERVOIR PARAMETERS

Yıldız, Tabiat Tan

Doctor of Philosophy, Petroleum and Natural Gas Engineering

Supervisor: Assoc. Prof. Dr. İsmail Durgut

July 2025, 70 pages

Sudden velocity changes—whether natural or operational—generate pressure surges that travel as waves through pipes. The best-known example is the water-hammer pulse produced by a sudden valve closure. In petroleum engineering, such transients have been analyzed to estimate flow rate, detect diameter restrictions, and identify wax, scale, or corrosion. More recently, researchers have shown that the same waves also contain information about near-wellbore reservoir properties.

This study models the surge created by rapid valve closure with a transient one-dimensional pipe-flow solver and couples it to both analytical and numerical representations of the reservoir. The framework captures single-phase oil, gas, and fractured formations by linking pressure and flux at the sand face. A finite-element implementation replaces earlier hybrid schemes, allowing pipe hydraulics and porous-medium flow to be solved simultaneously and thus representing pressure-wave behavior more accurately.

To improve data quality, the work also proposes relocating the fast-acting valve and quartz gauge down-hole, close to the perforations. This configuration minimizes signal attenuation, preserves high-frequency content, and enhances sensitivity to reservoir parameters.

Finally, sensitivity analyses examine how fluid compressibility, acoustic velocity, tubing geometry, fracture conductivity, and valve-closure timing influence the recorded response. Results demonstrate that the coupled model distinguishes subtle variations in both pipe conditions and reservoir behavior, providing a practical tool for down-hole diagnostics and reservoir characterization.

Keywords: Pipe flow, Valve closure event, Pressure wave propagation, Well Testing, Reservoir parameters.

ÖZ

KUYULARDA REZERVUAR PARAMETRELERİNİ TAHMİN ETMEK AMACIYLA VANA-KAPAMA İŞLEMLERİNE BAĞLI BASINÇ DALGALANMALARININ ANALİZİ

Yıldız, Tabiat Tan
Doktora, Petrol ve Doğal Gaz Mühendisliği
Tez Yöneticisi: Doç. Dr. İsmail Durgut

Temmuz 2025, 70 sayfa

Ani (doğal veya insan kaynaklı) hız değişimleri, kuyunun üretim borusu boyunca dalgalar hâlinde yayılan basınç atımlarına yol açar. Bunun en iyi bilinen örneği, vananın ani kapatılmasıyla oluşan su darbesi basınç dalgasıdır. Petrol mühendisliğinde bu geçici basınç sinyalleri; debi tahmini, boru içi daralma tespiti ve parafin, kireç ya da korozyon kaynaklı çap kısıtlarını belirlemek için kullanılmaktadır. Son yıllarda aynı dalgaların, kuyu çevresindeki rezervuar özellikleri hakkında da bilgi taşıdığı gösterilmiştir.

Bu çalışmada, ani vana kapatılmasıyla oluşan basınç dalgası bir boyutlu geçici boru akış modeliyle çözümlenmiş, ardından hem analitik hem de sayısal rezervuar temsilleriyle eşleştirilmiştir. Sandface (kuyu-rezervuar ara yüzü) basınç-akıs ilişkilendirmesi sayesinde tek fazlı petrol, gaz ve çatlaklı formasyon senaryoları modellenmiştir. Önceki hibrid (sayısal boru/analitik rezervuar) yaklaşımlar yerine

geliştirilen sonlu eleman şeması, boru hidrodinamiği ile gözenekli ortam akışını aynı anda çözerek basınç dalgası davranışını daha gerçekçi aktarmaktadır.

Veri kalitesini artırmak amacıyla, hızlı kapanabilen vana ile kuvars basınç sensörü yüzey yerine kuyu dibine—perforasyonlara yakın—yerleştirilmiştir. Bu düzenleme sinyal zayıflamasını azaltır, yüksek frekanslı içeriği korur ve rezervuar parametrelerine duyarlılığı yükseltir.

Ayrıca, akışkan sıkışabilirliği, akustik hız, boru geometrisi, çatlak iletkenliği ve vana kapama süresinin sinyal üzerindeki etkileri ayrıntılı hassasiyet analizleriyle incelenmiştir. Bulgular, geliştirilen eşleştirilmiş modelin hem boru koşullarındaki hem de rezervuar davranışındaki ince değişimleri ayırt edebildiğini göstererek yöntemin kuyu içi teşhis ve rezervuar karakterizasyonu için pratik bir araç sunduğunu ortaya koymaktadır.

Anahtar Kelimeler: Boru akışı, Vana kapama olayı, Basınç dalgası yayılımı, Kuyu Testi, Rezervuar Parametreleri.

To My beloved family

To My late father, Mr. Zeki Yıldız, whom I cherished more than life itself

ACKNOWLEDGMENTS

First and foremost, I would like to express my deepest gratitude to my supervisor, Assoc. Prof. Dr. İsmail Durgut, for his precious guidance, solid support, inspiration, and constant encouragement throughout the course of my research. His prudence and experience have greatly enriched my work, and I am truly thankful for his contributions and humanity.

Special thanks go to Asst. Prof. Dr. Mehmet Onur Doğan, Assoc. Prof Dr. Çağlar Sınayuç, Asst. Prof Dr. Gamze İpek and Prof. Dr. Murat Uysal as my PhD thesis committee members. Their technical expertise, collaborative personality, and continuous support have been essential in the completion of this research. I deeply appreciate their contributions and friendship.

I would also like to extend my sincere thanks to my friend Ahmet Ergun Mengen. His friendship and belief in me have provided courage I needed during the challenging times of my PhD journey.

Last but certainly not least, I would like to extend my heartfelt thanks to my dear wife Aysel. Her unconditional love, patience, and immense help have been my foundation and source of strength throughout this journey. Without my wife and my two sons Efe Tan and Ömer Tan continuous support, this achievement would not have been possible, and I would have stopped my efforts a long time ago.

Thank you all for being part of this incredible journey.

TABLE OF CONTENTS

ABSTRACT v

ÖZ vii

ACKNOWLEDGMENTS x

TABLE OF CONTENTS xi

LIST OF TABLES xiii

LIST OF FIGURES xiv

1 INTRODUCTION 1

2 LITERATURE REVIEW 5

3 STATEMENT OF THE PROBLEM 21

4 MATERIALS AND METHODS 23

4.1 Proposed New Test Configuration 23

4.2 Transient Pipe – Analytical Reservoir Model 24

4.2.1 Mathematical Model of Transient Flow of Fluid in Pipelines 25

4.2.2 Mathematical Modelling of Transient Flow of Fluid in Homogenous Porous Media 28

4.3 Numerical Solution Framework of Coupling and Solving Transient Porous Flow and Pipe Flow Models by Finite Element Model 29

4.4 Possible Field Test Configuration 31

4.4.1 Downhole Shut-in Tool 31

4.4.2 Downhole Pressure Measurement Gauge 33

5 RESULTS AND DISCUSSION 37

5.1 Testing and Comparison with Finite Element Model..... 37
5.2 Sensitivity Studies 42
6 CONCLUSION 63
REFERENCES 65
CURRICULUM VITAE 69

LIST OF TABLES

TABLES

Table 5-1 Model parameters 38

Table 5-2 Model parameters for sensitivity analysis in oil reservoir..... 43

Table 5-3 Model parameters for sensitivity analysis in gas reservoir..... 44

LIST OF FIGURES

Figure 2-1. Schematic of the tested well and estimated wax deposition along tubing 11

Figure 2-2. Pressure pulse response measured and simulated at the wellhead (before cleaning operation) 12

Figure 2-3. Inner diameter (flow diameter) of tubing: a) New tubing [ ] b) Wax-deposited tubing [ ] c) Cleaned tubing [ ] 14

Figure 2-4. Pressure pulse response measured and simulated at the wellhead (after cleaning operation) 16

Figure 2-5. Measured pressure pulse response the wellhead and simulated results using constant pressure boundary condition (after cleaning operation) 17

Figure 2-6. Measured pressure pulse response the wellhead and simulated results using reservoir boundary condition (after cleaning operation) 18

Figure 4-1. Schematic of the proposed well test setup. A rapid-closure sleeve valve and a high-resolution quartz gauge are positioned near the perforated interval. The sudden valve closure generates a water-hammer pulse that propagates upward in the tubing and interacts with the reservoir across the perforations. Symbols: P_r – far-field reservoir pressure; P_{bhf} – bottom-hole flowing pressure immediately above the perforations. 24

Figure 4-2. The discretization of the surge pipe-flow model and reservoir model . 31

Figure 4-3. The schematic of the downhole instand shut-in tool example 33

Figure 4-4. Schematic of the downhole quartz gauge assembly and sub components that is commonly used in industry 34

Figure 5-1. Valve closing period: Velocity at valve section vs. time 39

Figure 5-2. Pressure history at wellhead and bottom hole b) Presure distribution in reservoir obtained by COMSOL models 40

Figure 5-3. a) Pressure history at wellhead and bottom hole b) Presure distribution in reservoir obtained by CLAWPACK-based pipe models and analytical reservoir model..... 41

Figure 5-4. Sensitivity results in oil reservoir for oil types: a) Pressure recorded at valve location b) Pressure profile through reservoir..... 46

Figure 5-5. Sensitivity results in oil reservoir for oil rate: a) Pressure recorded at valve location b) Pressure profile through reservoir..... 47

Figure 5-6. Sensitivity results in oil reservoir for permeability: a) Pressure recorded at valve location b) Pressure profile through reservoir..... 49

Figure 5-7. Sensitivity results in oil reservoir for porosity: a) Pressure recorded at valve location b) Pressure profile through reservoir..... 50

Figure 5-8. Sensitivity results in oil reservoir for tubing length: a) Pressure recorded at valve location b) Pressure profile through reservoir..... 52

Figure 5-9. Sensitivity results in gas reservoir for rates: a) Pressure recorded at valve location b) Pressure profile through reservoir 53

Figure 5-10. Sensitivity results in gas reservoir for permeability: a) Pressure recorded at valve location b) Pressure profile through reservoir..... 54

Figure 5-11. Sensitivity results in gas reservoir for porosity: a) Pressure recorded at valve location b) Pressure profile through reservoir..... 55

Figure 5-12. Modelled reservoir and fracture schematic 56

Figure 5-13. Sensitivity results in fractured oil reservoir for fracture aperture: a) Pressure recorded at valve location b) Pressure profile through reservoir 59

Figure 5-14. Sensitivity results in fractured oil reservoir for fracture half length: a) Pressure recorded at valve location b) Pressure profile through reservoir 60

Figure 5-15. Sensitivity results in fractured oil reservoir for fracture permeability: a) Pressure recorded at valve location b) Pressure profile through reservoir 61

CHAPTER 1

INTRODUCTION

Water hammer, or hydraulic shock, is a pressure surge or wave caused by a sudden change in the velocity or direction of a flowing fluid. This phenomenon happens in pipeline systems for instance when a valve closes suddenly, sudden changes in flow rate or when a pump is rapidly shut down. The sudden deceleration or redirection of the fluid generates high-pressure waves, which may lead to serious consequences, such as structural damage to pipelines. On other hand, this specific pressure waves have also been used observation and estimation purposes in various engineering applications. Therefore, the phenomenon has been extensively studied for both liquid and gas flows, as the dynamics and propagation of pressure waves differ significantly between the two mediums.

The foundational understanding of water hammer dates back to the work of Joukowsky in 1898, who derived the fundamental equation relating the pressure surge to the fluid density, the wave speed, and the change in velocity. His approach provided a well-defined basis for analyzing transient pressure phenomena in incompressible fluids and became a foundation for the study of pressure wave mechanics. Joukowsky's work not only provided insights into the physical mechanisms of water hammer but also served as the basis for a wide range of theoretical and practical advancements in the field. Furthermore, his experimental study showed that water hammer waves propagate in the pipe system with a constant velocity that is independent of the power of shock wave but function of the thickness and material of pipe. Subsequent studies have expanded on this foundation to address complex systems, incorporating factors such as compressibility, pipe elasticity, and damping effects.

For the modelling of propagation of shock waves along piping systems, over the decades, various approaches were developed to simulate transient behavior of fluid

flow (gas and/or liquid phases) in pipes more accurately. Numerical modeling methods for simulating the propagation of pressure waves in piping systems were the main tools for understanding and modeling of the phenomenon. These models generally solve the one-dimensional (1D) transient flow equations, derived from the conservation of mass, momentum, and energy, using computational techniques such as the method of characteristics (MOC) or finite difference/finite volume methods. The MOC is widely used due to its accuracy in capturing shock wave propagation and its ability to handle complex boundary conditions. Finite difference and finite volume methods, on the other hand, offer flexibility in handling two- or three-dimensional geometries and transient scenarios. Advanced approaches, such as computational fluid dynamics (CFD), were also developed for detailed insights into the interaction of pressure waves with the bounding environment such as pipe walls, fittings, and flow control units.

From an operational perspective, water hammer and the resulting shock waves in pipeline systems may bring about significant operational challenges in the petroleum industry. These intense pressure waves can cause structural damage to pipelines, leading to ruptures, leaks, and environmental hazards. They also disrupt control instruments, impairing sensor accuracy and operational efficiency. High water hammer may destabilize sand, causing sand production that damages equipment and reduces productivity. Additionally, pressure surges can affect reservoir performance and well operations during injection or production cycles.

On the other hand, the water hammer phenomenon has also a few potential applications in the petroleum industry for observation and estimation purposes. It has been suggested to exploit it to estimate flow rate, flow area restrictions, some characteristics of flowing fluid and reservoir properties.

In industry widely used well testing operations provide parameters of reservoir fluid and rock characteristics. Well testing is a critical reservoir evaluation technique used to determine the dynamic properties of a reservoir and the performance characteristics of a well. By analyzing pressure and flow rate data obtained under controlled production or injection conditions, well testing provides valuable insights

into permeability, skin factor, reservoir boundaries, and fluid properties. The results support decision-making in reservoir management, field development planning, and production optimization. Proper design and execution of well tests ensure accurate interpretation, enabling operators to characterize near-wellbore conditions, identify formation damage, and estimate reservoir parameters with confidence.

This study investigates methods to estimate near wellbore reservoir properties by using the pressure waves created by rapid valve closure events. The analysis employs coupled transient models for pipe flow and reservoir behavior. The transient pipe flow models applied in this study are 1D finite element and finite volume techniques. The applied reservoir models are analytical solutions with simple initial and boundary conditions (that is, slightly compressible single-phase flow through porous media) and numerical models of slightly compressible and compressible fluid flow in porous media including fractured reservoirs. The pipe flow models capture the propagation of pressure waves, whereas the reservoir models are applied as a boundary condition to the pipe flow model which simulate the fluid flow in porous media as response to pressure transients reaching downhole. The coupled models are used to perform sensitivity analysis for reservoir, flowing fluid parameters.

CHAPTER 2

LITERATURE REVIEW

The relation between pressure surge or wave caused by a sudden change in the velocity or direction of a flowing fluid and velocity changes, was first stated by Joukowsky in 1898 [1]. It is defined as:

$$\Delta p_a = \rho \, c \, \Delta v, \tag{2.1}$$

where Δv is observed sudden velocity change in fluid flow along a pipe, ρ and c are density and speed of sound of the fluid at in-situ condition and Δp_a is expected therotical pressure change due to sudden velocity change called waterhammer pressure. The equation above is usually reffered as the "Joukowsky equation". However, it is also called as either the "Joukowsky-Frizell" or the "Allievi" equation because Frizell [2] and Allievi [3] also found the equation unaware of the achievements of one another.

However, Johannes von Kries was the first to set out a theory of water-hammer in 1883 while analysing arterial blood flow. In that work he derived the equation later known as the Joukowsky formula – fifteen years before Joukowsky and Frizell published their own versions in 1898 –. By factoring skin-friction into unsteady laminar flow, he obtained expressions for wave damping and line packing, and confirmed them with tests on rubber hoses. Von Kries then compiled the earliest textbook on what we now call classical water-hammer, published in 1892. [4]

Joukowsky provided a well-defined basis for analyzing transient pressure phenomena in incompressible fluids and became a foundation for the study of pressure wave mechanics. Joukowsky's work not only provided insights into the physical mechanisms of water hammer but also served as the basis for a wide range of theoretical and practical advancements in the field [5]. Furthermore, his experimental study showed that water hammer waves propagate in the pipe system with a constant velocity that is independent of the power of shock wave but function

of the thickness and material of pipe. Subsequent studies have expanded on this foundation to address complex systems, incorporating factors such as compressibility, pipe elasticity, and damping effects [6].

The phenomenon of water hammer and the subsequent propagation of generated shock waves in the pipe system have been studied for their operational impacts in the petroleum industry.

One of the primary operational impacts of water hammer is structural damage to the pipeline system. The intense pressure waves can cause significant stress on pipes, fittings, and joints, leading to cracks, fractures, or even complete pipeline failure. Wylie and Streeter [7] provides a comprehensive overview of fluid transients, including water hammer, and their effects on various systems, including those in the petroleum industry. This structural damage can result in leakage of hydrocarbons, posing environmental hazards and safety risks.

In addition to structural damage, water hammer can critically affect control and monitoring instruments. The sudden pressure surges can disrupt the calibration and functioning of sensors, gauges, and other monitoring equipment, leading to inaccurate readings and potential operational inefficiencies [8, 9, 10].

Another critical impact of water hammer is the risk of sand destabilization in water injection wells. The pressure waves can trigger sand liquefaction, causing sand particles to become suspended in the fluid flow [11] . This can lead to sand production, which can erode and damage downhole equipment, reduce well productivity, and increase maintenance costs [12].

Furthermore, water hammer can significantly affect the performance of injection and production wells. The pressure surges could influence reservoir performance and well productivity, particularly in scenarios involving injection or production cycles [13].

Beyond formation damage, water hammer has also been studied in the context of equipment dynamics. Livescu and Watkins [14] focused on the impact of water hammer-induced pulses on the radial vibrations of coiled tubing. They developed a

computational model to simulate the dynamic response of coiled tubing systems under these conditions, offering a predictive tool for managing potential failures and optimizing coiled tubing operations.

As explained above with examples, the water hammer phenomenon is often related with potential damage and operational issues in piping systems, it also presents several promising applications in the petroleum industry for observation and estimation purposes. In the literature, it has been suggested to utilize water hammer for estimation of various parameters, such as flow rates, flow area restrictions, characteristics of the flowing fluid, and reservoir properties. Valuable information about the behavior and characteristics of the system can be obtained by analyzing the pressure waves generated by sudden changes in fluid flow velocity.

One of the key components for understanding propagation of pressure wave (in particular, the water-hammer pressure) along flow conduits is developing an accurate mathematical and numerical model that accurately captures the underlying fluid dynamics and boundary interactions. Modeling water hammer involves solving transient flow equations derived from the principles of mass, momentum, and energy conservation. Over the decades, several numerical methods have been developed to simulate pressure wave propagation in pipelines, each with distinct advantages and limitations.

The Method of Characteristics (MOC) is one of the most widely used techniques for modeling water hammer due to its accuracy in capturing shock wave propagation and handling complex boundary conditions [5]. MOC transforms the partial differential equations (PDEs) governing transient flow into ordinary differential equations along characteristic lines, enabling precise tracking of pressure waves. MOC is effective in simulating fluid transients in pipelines, including petroleum systems [7]. However, MOC is primarily suited for one-dimensional (1D) systems and becomes computationally intensive for two- or three-dimensional geometries.

Finite difference and finite volume methods offer flexibility in modeling transient flows across various geometries. Finite difference methods discretize the governing

PDEs on a grid, approximating derivatives with difference equations. While versatile, they are prone to numerical diffusion, which can reduce accuracy in capturing sharp pressure fronts [5]. Finite volume methods, on the other hand, conserve mass, momentum, and energy by integrating the governing equations over control volumes, making them more stable for complex systems.The finite volume method implemented in CLAWPACK (Conservation LAWs PACKage) is particularly relevant to this study. CLAWPACK is a Fortran-based solver library designed for hyperbolic systems of conservation laws, such as those governing transient pipe flow [15, 16]. It employs Riemann solver methodology to handle discontinuities in pressure and velocity, ensuring robust simulation of shock wave propagation. LeVeque (2002) [17] introduced CLAWPACK as a versatile tool for solving 1D, 2D, and 3D hyperbolic PDEs, with applications in fluid dynamics, acoustics, and geophysics. In petroleum engineering, CLAWPACK has been used to model pressure transients in pipelines, as demonstrated by Bale et al. (2002), who applied it to simulate wave propagation in gas pipelines [21]. The library's ability to handle time-dependent boundary conditions, such as valve closures, makes it well-suited for water hammer analysis. However, CLAWPACK's computational cost increases with grid refinement, and its application to coupled pipe-reservoir systems requires careful integration with reservoir models.

Computational Fluid Dynamics (CFD) provides detailed insights into water hammer by solving the full Navier-Stokes equations in three dimensions. CFD can model complex interactions between pressure waves and pipe walls, fittings, and multiphase flows [10]. Messahel et al. [8] used CFD to study fluid-structure interactions in water hammer events, highlighting its ability to capture secondary effects like pipe vibrations. However, CFD's high computational cost and requirement for specialized expertise limit its practical use in routine reservoir engineering applications.

Water hammer can be utilized to estimate flow rates by observing the pressure wave propagation and its interaction with the pipeline system. Gudmundsson and Celius [18] suggested the use of water hammer pressure waves for estimation of flow rates.

The pressure waves can also help to identify flow area restrictions, such as blockages or deposits and to estimate the location and size of restrictions in pipelines, by analyzing changes in wave behavior. Gudmundsson et al. [19] elaborated the technique using water hammer pressure waves to detect pipeline deposits.

Pressure waves from water hammer events can be used for leak detection and evaluating pipeline condition [20, 21]. Besancon and Georges [20] proposed an orthogonal collocation (OC) scheme to obtain a compact, low-order model of the water-hammer equations for pressurized pipelines. Unlike conventional finite-difference methods, the OC approach discretizes the spatial domain at selected nodes, yielding an ordinary-differential system that captures point-wise pressure and flow dynamics and can explicitly embed leaks as boundary conditions. Simulation shows the OC model matches finite-difference results while offering lower computational cost and clearer leak signatures. An observer based on an extended Kalman filter successfully estimates leak position and magnitude, demonstrating the model's potential for real-time leak detection in pipelines. Ayed et al. [21] investigated leak detection in pressurized pipelines by analyzing water-hammer waves in both elastic and viscoelastic pipes. A one-dimensional continuity–momentum model is solved via the method of characteristics; leaks are represented as orifices and treated as internal boundaries. Pressure signals at the valve are examined in the time domain (arrival and amplitude of leak-reflected waves) and in the frequency domain (shifts in resonant-peak spacing). Numerical tests show that the time-domain method locates leaks within ≤2 % error for elastic pipes and ≤8 % for viscoelastic ones, while frequency analysis is less accurate but still practical.

One other application of pressure wave could be to utilize it as a rapid well-testing technique for estimating key reservoir parameters. Well testing [22] is a vast discipline that traditionally relies on controlled flow-rate changes—such as drawdown, buildup, or injection/falloff sequences—and hours or days of pressure monitoring to infer permeability, skin factor, and boundaries. Incorporating well test data into integrated reservoir characterizations may require the well test to be modeled in a reservoir simulator that also forward simulates other dynamic data

being matched. Standard finite-difference reservoir simulators use the Peaceman well index, which is based on the solution to single-phase, steady-state, incompressible flow. For a pressure transient test the assumptions of steady-state, incompressible flow is not applicable. However, instead of modifying the well index it is common to account for this by using highly refined grids around wells and making very careful choices of timestep sizes to model well tests. Archer and Yildiz [23] focused a new well index formulation that allows well tests to be simulated accurately in finite difference simulators using uniform, relatively coarse grids, without the problem of artifact wellbore storage (early time unit slope on the pressure derivative only) that otherwise occurs. The well index model computes the average pressure in the well block directly from the analytical solution for infinite acting radial flow. They developed transient well index can be readily incorporated into a simulator. Similarly, a water-hammer pulse produced by a valve closure generates a high-frequency pressure signal that interrogates the near-wellbore region within seconds. It may provide valuable information about reservoir properties, such as permeability, porosity, fracture parameters and pressure, by examining the propagation and reflection of pressure waves caused by abrupt changes in flow conditions. Carey et al. [24] suggested that hydraulic fracture parameters could be estimated from the water hammer pressure signature by using a transient pipe flow model.

Recently, Durgut et al. [25] proposed that the pressure waves generated from valve closure event can be used to estimate reservoir parameters, the transmissivity and storativity in the near-wellbore region which are defined as function of the permeability, thickness, compressibility, porosity, and viscosity data specific to the formation and fluid in the well:

Transmissivity:
$$T = \frac{kh}{\mu} \tag{2.2a}$$

Storativity:
$$S = \phi c_t h \tag{2.2b}$$

The idea that reservoir parameters could be found with water hammer pressure waves was indeed first noticed while working on another study. This study was to estimate the location and size of wax deposition occurred in a tubing string using pressure-pulse method. The data used to test this method was a data set obtained from a single-phase oil production well producing from a deep carbonate reservoir. The well was 5500 meters deep. Telescopic tubing string was installed in the well as shown in Figure 2-1. The nominal diameter of the 1675-meter upper section of the tubing string was 3½ inches, and the nominal diameter of the lower section was 2⅞ inches. The inner diameters corresponding to these nominal diameters were 74.2 mm and 59 mm, respectively. Wax deposition was reported in this well.

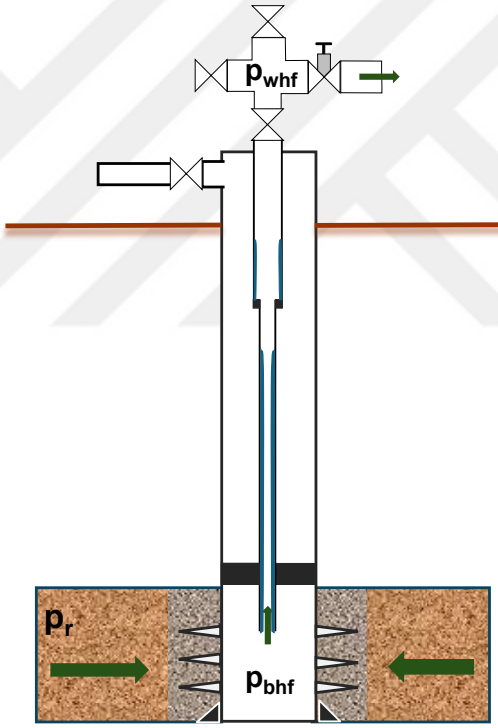

Figure 2-1. Schematic of the tested well and estimated wax deposition along tubing

Tubing string cleaning workover operation was planned in this well, therefore, the pressure-pulse method was applied in this well before and after the cleaning operation to show the effect of the method. The data set to be discussed first belongs to the situation before the workover operation.

While production was continuing in the well, the well was shut-in by closing the master valve at the wellhead very quickly. The wellhead pressure was observed by recording the wellhead pressure 40 seconds starting just before closing event. The recording system was capable of saving data at 1000 Hz. The data was down-sampled from 1000 data per second to 10 data per second by a digital filtering method. Figure 2-2 shows the data recorded at the wellhead pressure for the first 15 seconds during which the reflection from the bottom hole was observed.

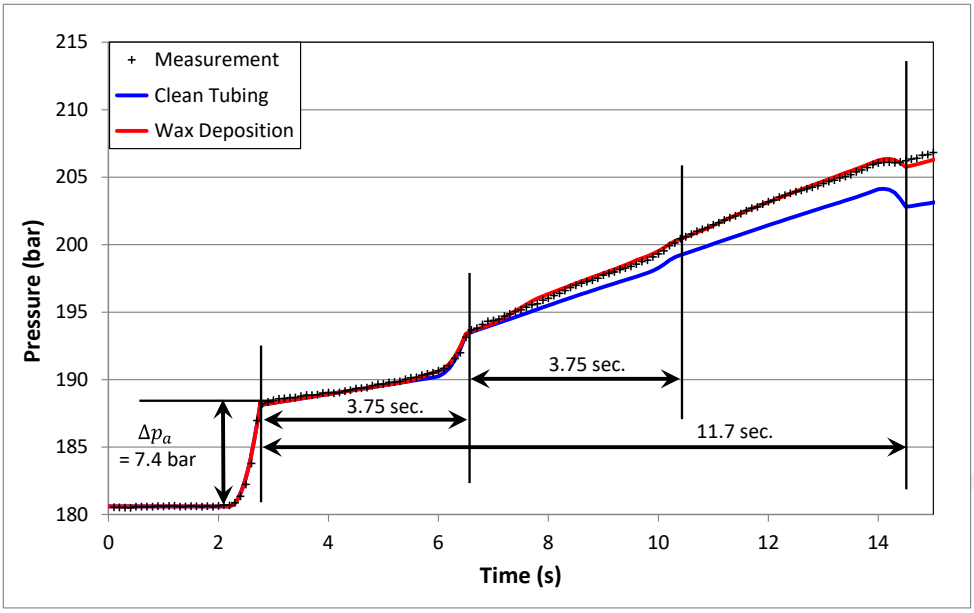

Figure 2-2. Pressure pulse response measured and simulated at the wellhead (before cleaning operation)

In the test data, the water hammer pressure (Δp_a) that occurs as a result of full valve closing in approximately 0.5 seconds is clearly observed. This pressure wave reflects first at the tubing diameter change and then from the bottom hole. The first reflection was observed 3.75 seconds later (see Figure 2-2) after the valve was fully closed. It comes from the tubing diameter change. This reflection was repeated once more, which was weakened. Then, 11.70 seconds later, the reflection from the bottom hole appears.

Using the reflections from the diameter changes (i.e. 3.75 seconds), the average acoustic velocity for the upper section of the tubing string can be calculated as 893

m/s and for the entire well length (surface to bottom) as 940 m/s. After calculating the average speed of sound and accepting the calculated values as the speed of sound values at the average distance of each section, one can obtain the speed of sound profile. Assuming a linear profile, the speed of sound at the surface was estimated to be 873 m/s and 1008 m/s at the bottom of the well.

The oil density is determined using PVT modeling methods, with a value of 709 kg/m^3 at the wellhead flow conditions (181 bar, 100°C) and 695 kg/m^3 at the bottom of the well (585.2 bar, 170°C). The density profile along the well was assumed to vary linearly with distance from the wellhead.

As stated earlier in the Joukowsky equation (Eq. 2.1), it is defined as $\Delta p_a = \rho v c$. The magnitude of the water hammer pressure is equal to the product of the acoustic velocity c, the density of the flowing fluid ρ, and the flow rate of the fluid v. Since the mass flow rate in a pipe with cross-sectional area A is $m = \rho v A$, one can find the mass flow rate using the Joukowsky equation from the following relationship:

$$m = \frac{\Delta p_a A}{c} \tag{2.1}$$

What is required is the sound velocity and water hammer pressure measurements at the point and time when the valve is closed. The water hammer pressure in the performed test was 7.4 bar, the sound velocity at the well head condition was 873 m/s and the pipe cross-sectional area was 43.24 cm^2 (the pipe inside diameter was 7.42 cm). According to these values, the mass velocity can be calculated as 3.66 kg/s.

Using the "mass rate" obtained from the Joukowsky equation above with the well and fluid properties mentioned above, a simulation can be performed by using the transient pipe flow model described earlier. In this simulation, if the tubing were completely new and clean (see the blue line in Figure 2-3), the wellhead pressure record shown as the blue line in Figure 2-2 can be obtained.

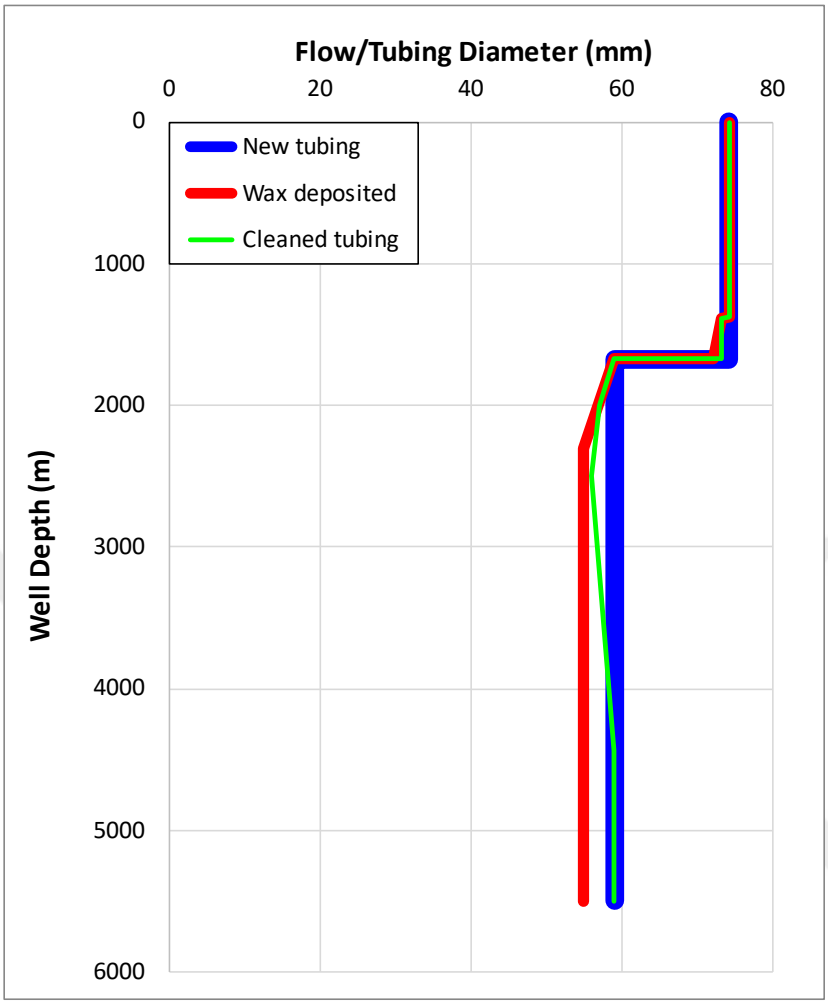

Figure 2-3. Inner diameter (flow diameter) of tubing: a) New tubing [ ] b) Wax-deposited tubing [ ] c) Cleaned tubing [ ]

As seen in the figure, the simulation results are quite different from the measurements. This situation actually indicates the wax deposition that has occurred in the tubing. As a result of the experimental simulations and matching studies, it was estimated that there was a 1 mm wax deposition (i.e. a total decrease of 2 mm in pipe diameter) in the last 300 meters of the larger diameter tubing (3½ inches tubing string), and in the 2⅞ inch lower section, starting from where the smaller diameter tubing was installed, there was a gradually increasing up to 2 mm of deposition in the first 600 meter and this 2 mm wax deposition (a total decrease of 4 mm in pipe diameter) extends to the bottom of the well. When simulations were

performed with this assumed wax deposition (see the red line in Figure 2-3), the results matched the measurements quite well as shown in Figure 2-2.

The same analysis and observations were also made for the same test after a workover operation to clean tubing string from wax deposition. Figure 2-4 shows the data recorded at the wellhead pressure for the first 15 seconds during which the reflection from the bottom hole was observed.

In this test, the water hammer pressure (Δp_a) wave reflects first at the tubing diameter change and then from the bottom hole. The first reflection was observed 3.55 seconds later after the valve is fully closed. It comes from the tubing diameter change. This reflection was repeated once more, which was weakened. Then, 11.30 seconds later, the reflection from the bottom hole appears. Using the reflections from the diameter changes (i.e. 3.55 seconds), the average acoustic velocity for the upper section of the tubing string can be calculated as 943 m/s and for the entire well length (surface to bottom) as 973 m/s. The same analysis done for the test before cleaning operation can also be done. After calculating the average speed of sound and accepting the calculated values as the speed of sound values at the average distance of each section, one can obtain the speed of sound profile. Assuming a linear profile, the speed of sound at the surface was estimated to be 930 m/s and 1016 m/s at the bottom of the well. Since the pressure at the bottom hole should be almost the same and the wellhead pressure was slightly different from the previous test condition, the PVT modeling gives almost the same density profile: 710 kg/m^3 at the wellhead flow conditions and 695 kg/m^3 at the bottom of the well.

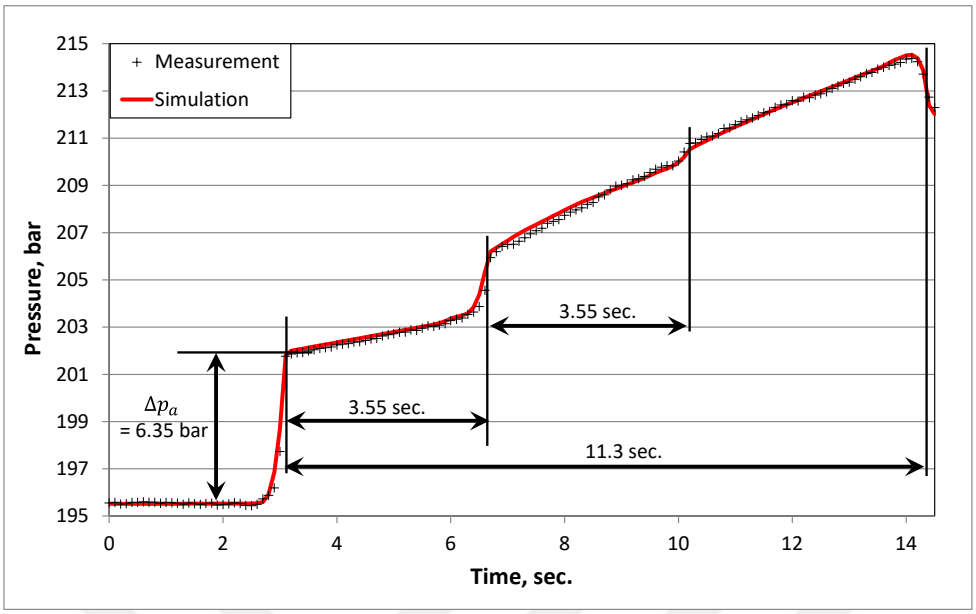

Figure 2-4. Pressure pulse response measured and simulated at the wellhead (after cleaning operation)

The water hammer pressure in this test was 6.35 bar, the sound velocity at the well head condition was 930 m/s and the pipe cross-sectional area was 43.24 cm^2. According to these values, the mass velocity can be calculated as 2.95 kg/s.

Simulations were conducted using the mass rate calculated above and the determined fluid properties. Starting from the "wax deposition" identified using the previous test and analysis, and assuming that the deposited material should be removed after workover operation; series of simulations were carried out with different deposition profiles to estimate the flow diameter profile. These trial-and-error matching studies resulted in the profile shown by the green line of Figure 2-3. Again, the simulated wellhead pressure matched the measurements very well as shown in Figure 2-4.

The two sets of simulation results above demonstrate that the developed transient flow model matches very well with the measured data. This indicates that the mathematical model accurately reflects reality. One of the key requirements of such mathematical models is the boundary conditions. In this model, it was assumed that the pressure at the bottom of the well remains constant. This assumption produced results consistent with reality in both cases as shown in Figure 2-2 and Figure 2-4.

In the second test, pressure measurements were conducted in the well not only for the 10–15 seconds which was necessary for deposition detection but indeed for a longer duration (see Figure 2-5).

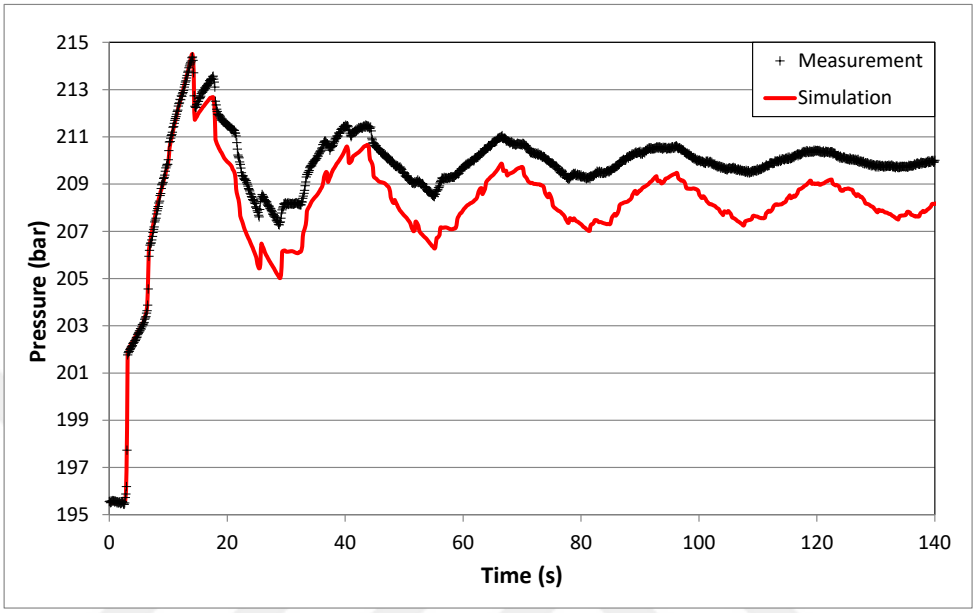

Figure 2-5. Measured pressure pulse response the wellhead and simulated results using constant pressure boundary condition (after cleaning operation)

When the simulation in the second analysis was extended to a longer period, a significant discrepancy was observed between the measurements and the simulation results. This clearly indicates that the applied “boundary condition” is inadequate and that a different boundary condition must be established for longer-term simulations.

The observed difference is clearly a result of the assumed constant pressure boundary condition. This type of boundary condition implies that the reservoir at the bottom of the well has infinite hydraulic capacity, meaning the pressure remains unchanged regardless of the amount of flow entering or leaving the well. However, in reality, the reservoir does not have infinite capacity, and the flow rate is dependent on the reservoir properties.

To model this behavior, they introduced an analytical reservoir model which is a function of two parameters, transmissivity and storativity (given in Eq's. 2.2 a and b) and coupled with their transient pipe flow model.

By iteratively adjusting the parameters transmissivity and storativity to match measured and simulated pressure data, the authors estimated reservoir parameter, the transmissivity and storativity as 25 D-m/cp and 4×10^{-4} m/bar, respectively. These values provide good matches with the measured data as shown in Figure 2-6.

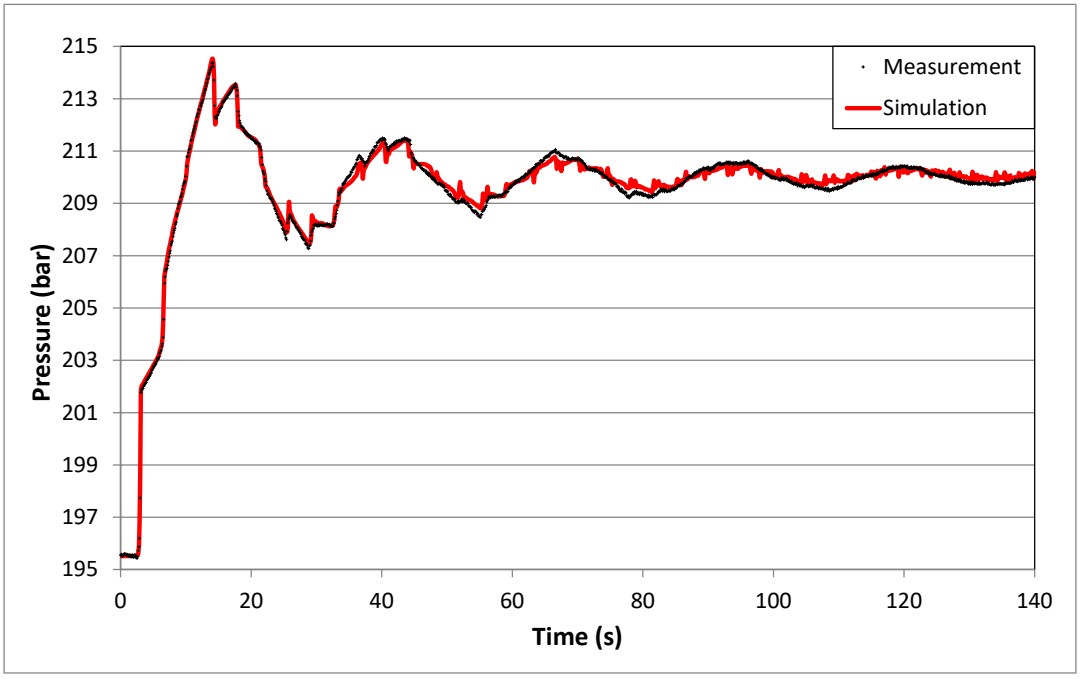

Figure 2-6. Measured pressure pulse response the wellhead and simulated results using reservoir boundary condition (after cleaning operation)

Although no particular values have been reported for the individual reservoir and fluid parameters, the reasonable ranges of the parameters may give the estimated transmissivity and storativity values. The reservoir where these tests were performed is carbonate reservoir with a thickness of 20 to 50 m. The reservoir is also known to produce light oil which has 0.2 to 1 cp viscosity at the reservoir and producing conditions. Moreover, a reasonable permeability range of 50 to 500 mD in a carbonate rock could have been assumed for the purposes of the well-test interpretation. When this permeability interval (50–500 mD) is combined with the

20–50 m net pay and the in-situ oil viscosity of 0.2–1 cp, it translates to a transmissivity on the order of 10^3–10^5 mD m /cp (or 1–100 D m /cp). Such values lie comfortably within the range reported for light-oil carbonate reservoirs of comparable thickness. If one further adopts typical carbonate porosities of 5–20 % and a total compressibility around $c_t = 1\times10^{-4} – 4\times10^{-4}$ bar^{-1}, net reservoir thickness of 20–50 m, the implied storativity falls between 1×10^{-4} m/bar and 4×10^{-3} m/bar, providing a coherent consistency check on the estimated reservoir parameters.

Few studies have been found in the literature coupling pressure surges in pipes with reservoir flow using different approaches.

Adiputro et al. [26] analyzed injection fall-off tests in geothermal wells where rapid valve closure triggers water-hammer transients. A coupled wellbore–reservoir model solves one-dimensional compressible flow in the well and radial heat- and mass-flow in the formation. Simulations reproduce field pressure traces that display an initial water-hammer spike followed by a diffusion-controlled decline. Results show that ignoring the early spike can misestimate transmissivity and storativity by up to 40 %. Incorporating the water-hammer segment improves parameter uniqueness and reveals near-wellbore damage zones. The workflow offers a fast, physics-based alternative to conventional fall-off interpretation for high-enthalpy geothermal systems.

In 2025, Deng et al. [27] proposes a diagnostic workflow that turns the high-frequency water-hammer pressure recorded immediately after fracturing shut-in. First, noise-filtered analysis of the wellhead signal helps to detect how many clusters actually fractured and where they are along the wellbore. These locations are given to a resistance-capacitance-inertance (RCI) representation that couples the wellbore and multiple fractures model, explicitly accounting for fluid leak-off, interactions with natural fractures. The transient water-hammer is then simulated by solving continuity and momentum equations with the method of characteristics and iteratively matching RCI parameters to the measured trace; fracture half-length, width and height are back-calculated from the matched RCI values. Model components were validated separately: (i) artificial signals showed fracture locations

were resolved within ±10 m; (ii) the water-hammer solver matched Fluent CFD results to within 0.26 MPa; (iii) fracture dimensions predicted for published field cases were within 6.5 % in length and 20 % in height of microseismic estimates. Sensitivity studies reveal that staged pump-shutdowns lengthen the useful water-hammer record while avoiding damaging pressure surges; more perforation clusters or denser natural fractures shorten each fracture. A shale-well case from the Sichuan Basin confirmed only three of six designed clusters propagated; the model's equivalent fracture of 448 m × 70 μm × 35 m agreed well with microseismic data and suggested the inactive clusters. Overall, the workflow extends water-hammer analysis to complicated, naturally fractured conditions and offers applicable guidance for stage design and shut-in practices.

CHAPTER 3

STATEMENT OF THE PROBLEM

When a valve in a pipeline closes suddenly, it creates pressure waves which are indeed very short and quick pressure transients and they propagate through the fluid. These waves can cause problems like pipeline damage and operational disruptions. However, they can also be used to estimate important reservoir and flow properties such as flow velocity, acoustic velocity, permeability, porosity, reservoir thickness.

The current method for analyzing these waves employs numerical pipe flow models and analytical reservoir models and do not fully capture how the pressure waves interact with different reservoir conditions for cases other than slightly compressible and infinite acting reservoir.

First of all, this study aims to solve these issues by developing numerical finite element models for both pipeline flow and reservoir behavior and coupling them. These developed models simulate how pressure waves travel and interact with reservoirs, helping to reflect the effect of key reservoir properties more accurately.

Then, the study introduces an improved testing approach that the valve closure event and the pressure measurements might be done in downhole instead of wellhead.

Afterwards, the developed models are used to perform sensitivity analysis for examining the effects of several governing conditions and parameters such as fluid properties, pipe configuration, characteristics of valve close event on reservoir response behavior.

CHAPTER 4

MATERIALS AND METHODS

This chapter, first, describes the test configuration proposed in the present work which introduces an improved testing approach that the valve closure event and the pressure measurements might be done downhole instead of wellhead. After introducing this down-hole configuration, the chapter revisits the modelling approach developed in earlier work. That simulator combining a transient pipe-flow solver with an analytical solution for the reservoir. The coupled numerical pipe/analytical reservoir model was first adopted for application of downhole valve and measurement. This simulator is actually used only for verification of the fully numerically developed model by finite element technique against the hybrid analytical/numerical models. Finally, the chapter presents the fully numerical model created for this study. Using finite-element methods, it solves the unsteady flow inside the tubing and the changing pressure in the porous media simultaneously. By introducing complete numerical framework allows to model compressible flow (gas reservoir) and fractured reservoirs which were not possible with the previous model.

4.1 Proposed New Test Configuration

The study introduces a down-hole testing scheme in which both the rapid valve-closure event and the high-frequency pressure measurements are performed near the reservoir depth rather than at the wellhead (Figure 4-1). Locating the shut-in tool and quartz gauge close to the sand-face minimises signal attenuation, enhances the sensitivity of the response to near-wellbore reservoir properties.

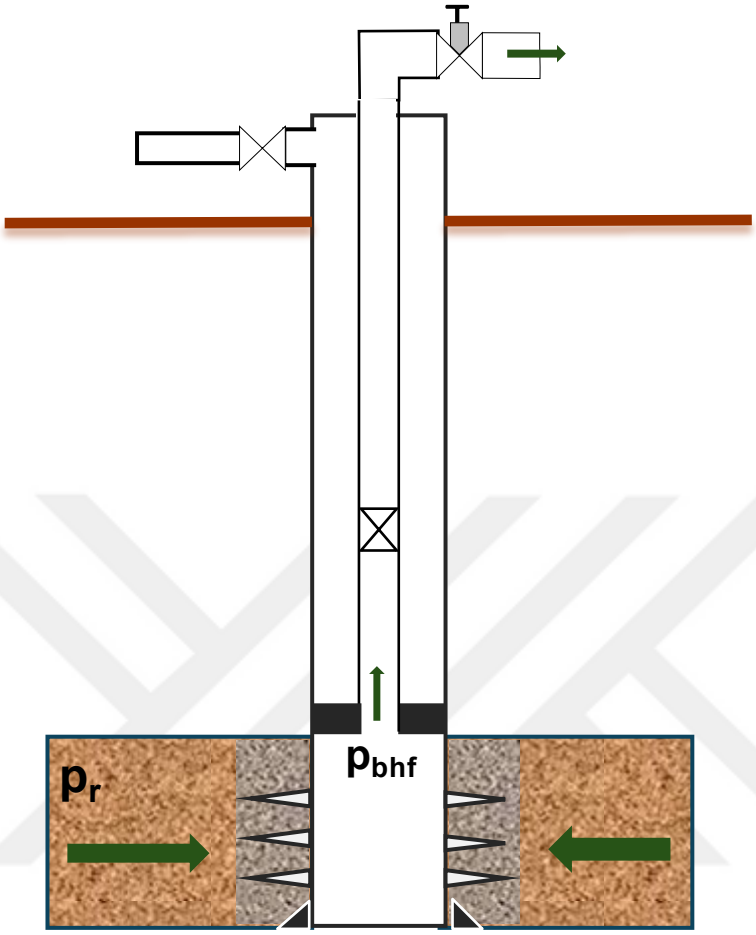

Figure 4-1. Schematic of the proposed well test setup. A rapid-closure sleeve valve and a high-resolution quartz gauge are positioned near the perforated interval. The sudden valve closure generates a water-hammer pulse that propagates upward in the tubing and interacts with the reservoir across the perforations. Symbols: P_r – far-field reservoir pressure; P_{bhf} – bottom-hole flowing pressure immediately above the perforations.

4.2 Transient Pipe – Analytical Reservoir Model

The original modeling approach brings together two components: a fully time-dependent numerical pipe-flow solver that tracks pressure waves along the tubing, and an analytical solution that describes how the reservoir responds to pressure-velocity changes after valve closing event.

4.2.1 Mathematical Model of Transient Flow of Fluid in Pipelines

The transient flow of fluid through pipelines is mathematically represented by a set of partial differential equations (PDEs). These equations describe the mass and momentum conservation for one-dimensional, transient, single-phase viscous fluid flow in a pipe. The equations are expressed as follows:

Mass Conservation:

$$\frac{\partial(A\rho)}{\partial t} + \frac{\partial(A\rho v)}{\partial x} = 0 \tag{4.1}$$

Momentum Conservation:

$$\frac{\partial(A\rho v)}{\partial t} + \frac{\partial(A\rho v|v|)}{\partial x} + \frac{\partial(Ap)}{\partial x} = -\frac{f}{2D}\rho v|v|A + \frac{3}{4}\frac{\partial}{\partial x}\left(A\mu\frac{\partial v}{\partial x}\right) - A\rho g\frac{dz}{dx} \tag{4.2}$$

Here, $v(x,t)$ is the cross-sectional average velocity, $p(x,t)$ is the pressure, $\rho(x)$ is the fluid density, and μ, $D(x)$ and $A(x)$ are the fluid's dynamic viscosity, flow diameter, and flow area, respectively. The term g represents gravitational acceleration, and z denotes the elevation in the opposite direction of gravity. These equations assume isothermal conditions, excluding the energy balance equation as heat transfer is negligible.

Simplifications and Sound Speed:

Pressure waves generated by sudden flow changes propagate with the in-situ speed of sound as a function of pressure, given by:

$$c(p) = \sqrt{\left(\frac{\partial p}{\partial \rho}\right)_s} \tag{4.3}$$

Using the sound speed definition and introducing the mass flow rate $m = \rho v A$ and neglecting the viscous term, the equations simplify to:

Simplified Momentum Conservation:

$$\frac{\partial m}{\partial t} + \left(1 - \left(\frac{v}{c}\right)^2\right)A\frac{\partial p}{\partial x} + 2v\frac{\partial m}{\partial x} = -\frac{f}{2DA}\frac{m|m|}{\rho} - A\rho g\frac{dz}{dx} \tag{4.4}$$

The viscous term is omitted as it is much smaller than other terms in transient flow conditions.

Simplified Mass Conservation:

$$\frac{\partial p}{\partial t} + \frac{c^2}{A}\frac{\partial m}{\partial x} = 0 \tag{4.5}$$

The system of equations given above can also be expressed in matrix form:

$$\frac{\partial \mathbf{q}}{\partial t} + \mathbf{B}\frac{\partial \mathbf{q}}{\partial x} = 0 \tag{4.6}$$

or, more compactly:

$$\mathbf{q}_t + \mathbf{B}\mathbf{q}_x = \mathbf{S} \tag{4.7}$$

Here, $\mathbf{q}$ represents the vector of state variables, $\mathbf{B}$ is the coefficient matrix for the spatial derivatives of these variables, and $\mathbf{S}$ is the "source term" representing external or continuous variations in the system. For the specified equations, these components are defined as:

$$\mathbf{q} = \begin{bmatrix} m \\ p \end{bmatrix}, \quad \mathbf{B} = \begin{bmatrix} 1-(v/c)^2 & 2v \\ 0 & c^2 \end{bmatrix}, \quad \mathbf{S} = \begin{bmatrix} -\frac{f}{2DA}\frac{m|m|}{\rho} - A\rho g\frac{dz}{dx} \\ 0 \end{bmatrix}. \tag{4.8}$$

The transient pressure pulse in the tubing is solved with CLAWPACK (Conservation LAWs PACKage) [16], a finite-volume code designed for time-dependent hyperbolic systems in one, two, or three spatial dimensions.

The pipe flow equation can be described one-dimensional hyperbolic equation having the form as follows:

$$\frac{\partial}{\partial \mathrm{t}}\left[\,\kappa(\mathrm{x})\;\mathrm{q}(\mathrm{x},\mathrm{t})\right] + \frac{\partial}{\partial \mathrm{x}}\,\mathrm{f}\,(\mathrm{q},\mathrm{x},\mathrm{t}) = \;\psi(\mathrm{q},\mathrm{x},\mathrm{t}) \tag{4.9}$$

Here q is the vector of conserved variables, κ(x) is a storage coefficient, f is the physical flux, and ψ collects source terms such as gravity or friction.

When κ = 1 and f depends only on q, Eq. (4.9) reduces to the conservative form

$$\frac{\partial \mathrm{q}}{\partial \mathrm{t}} + \frac{\partial \mathrm{f(q)}}{\partial \mathrm{x}} = 0 \tag{4.10}$$

Here, q represents the vector of state variables.

CLAWPACK can solve also hyperbolic equations that are not in conservation form,

$$\mathrm{q}_t + \mathfrak{B}(x,t)\mathrm{q}_x = \mathcal{S} \tag{4.11}$$

Finite-volume schemes advance each cell by solving a local Riemann problem at every cell face. Given left and right states $\mathrm{q_L}$ and $\mathrm{q_R}$, the solver decomposes their difference into elementary waves $\mathcal{W}^p$:

$$\mathrm{q_L} - \mathrm{q_R} = \sum\nolimits_p \mathcal{W}^p \tag{4.12}$$

For pipe flow the two eigen-speeds are typically $\lambda = \mp c$, where c is the local acoustic velocity.

With the wave fluctuations the first-order Godunov update reads

$$\mathrm{q}_i^{n+1} = \mathrm{q}_i^n - \frac{\Delta t}{\Delta x}[\mathfrak{B}^+ \Delta \mathrm{q}_i + \mathfrak{B}^- \Delta \mathrm{q}_{i+1}] \tag{4.13}$$

The Riemann solver should provide left and right going fluctuations respectively, $\mathfrak{B}^- \Delta \mathrm{q_i}$ and $\mathfrak{B}^+ \Delta \mathrm{q_i}$.

To sharpen discontinuities CLAWPACK adds a limited high-order correction Φ:

$$\mathrm{q}_i^{n+1} = \mathrm{q}_i^n - \frac{\Delta t}{\Delta x}[\mathfrak{B}^+ \Delta \mathrm{q}_i + \mathfrak{B}^- \Delta \mathrm{q}_{i+1}] - \frac{\Delta t}{\Delta x}[\Phi_{i+1} - \Phi_i] \tag{4.14}$$

Source term includes gravity and Darcy–Weisbach friction. The local sound speed $c(p)$ is recomputed every time step from its pressure dependence relation which was enhanced over earlier version of the model.

4.2.2 Mathematical Modelling of Transient Flow of Fluid in Homogenous Porous Media

The reservoir flow model is based on horizontal radial flow within a homogeneous porous medium filled with a slightly compressible fluid. It assumes isotropic and constant permeability and uniform reservoir thickness open to flow completely. Under these assumptions, combining the continuity equation with the Darcy Law and the Equation of States (EOS) one can derive an equation, which describes the pressure at any time at any radial distance in the porous medium: the well-known general diffusivity equation in radial geometry.

$$\frac{1}{r}\frac{\partial}{\partial r}\left(r\frac{\partial p}{\partial r}\right) = \frac{\phi\mu c_t}{k}\frac{\partial p}{\partial t} \tag{4.15}$$

The diffusivity equation can be expressed in dimensionless form by defining the dimensionless variable as follows:

Dimensionless time: $$t_D = \frac{k}{\phi\mu c_t r_w^2}t \tag{4.16a}$$

Dimensionless radius: $$r_D = \frac{r}{r_w} \tag{4.16b}$$

Dimensionless pressure: $$p_D(r_D, t_D) = \frac{2\pi kh}{q\mu}\left(p_i - p_{r,t}\right) \tag{4.16c}$$

where $p_{r,t}$ is the pressure at radius r and time t, r_w is the radius of wellbore, q is the volumetric flow rate at reservoir condition, p_i is the initial reservoir pressure. Using these variables, Eq. 4.15 becomes

$$\frac{1}{r_D}\frac{\partial}{\partial r_D}\left(r_D\frac{\partial p_D}{\partial r_D}\right) = \frac{\phi\mu c_t}{k}\frac{\partial p_D}{\partial t_D}. \tag{4.17}$$

For an infinite-acting reservoir, one can obtain the following exponential integral solution to the dimensionless diffusivity equation given above.

$$p(r,t) = p_i - \frac{q\mu}{2\pi kh}Ei\left(\frac{r_D^2}{4t_D}\right). \tag{4.18}$$

The solution to the diffusivity equation corresponding to time-varying flow rate can be obtained by applying the principle of superposition in time. The method is indeed to combine solutions to the diffusivity equation for discrete flow rate changes linearly to obtain the general solution to any flow rate history.

4.3 Numerical Solution Framework of Coupling and Solving Transient Porous Flow and Pipe Flow Models by Finite Element Model

The transient pipe flow model and the transient flow through porous media are coupled and solved by a Finite Element Modelling tool which allows to model and solve complex problems involving coupled physical phenomena across various fields. Coupling the numerical 1D transient pipe-flow model with analytical 1D reservoir model requires to combine 1D pipe-flow model 3D numerical porous media flow so that we can analyze the effects of inhomogeneities in reservoir, e.g. compressibility effect, different permeability distributions and fracture distributions on pressure changes following valve closure.

Under the assumptions of isothermal flow conditions, circular constant inner diameter pipe, the conservative balance laws simplify to a coupled system of mass and momentum balance equations.

The mass balance equation:

$$\frac{A}{c^2}\frac{\partial p}{\partial t} + \frac{\partial (A\rho \boldsymbol{u})}{\partial x} = 0 \tag{4.19}$$

The momentum balance equation:

$$\frac{\partial (A\rho \boldsymbol{u})}{\partial t} + \frac{\partial (A\rho \boldsymbol{u^2})}{\partial x} = -A\frac{\partial p}{\partial x} - \rho A g \sin\theta - f\frac{\rho |\boldsymbol{u}|(\boldsymbol{u})A}{2D} \tag{4.19}$$

where f is Darcy-Weisbach friction factor, D and A are the hydraulic diameter and area of pipe respectively. ρ and c are calculated from an equation of state.

The flexibility of the General (Coefficient) Form PDE interface of COMSOL helps to solve this system.

Flow equations for reservoir:

Mass balance:

$$\nabla(\rho \boldsymbol{u}) = Q_m, \tag{4.20}$$

where ρ is density, u is Darcy velocity, Q_m is source/sink term.

Momentum balance (Darcy flow):

$$\boldsymbol{u} = -\frac{K}{\mu}\nabla(p). \tag{4.21}$$

K is permeability, μ is dynamic viscosity.

The coupling between the models is established with pressure and flux continuity. The coupling strategy is explicit in time. Within single time step first the reservoir model is run for a given well rate and the pressure distribution in reservoir is solved. Then, the sand face pressure is given as boundary condition to the surge pipe flow model and pressure and velocity distribution in the well is solved. The velocity at the sand face node of the pipe flow is given as rate boundary condition for the reservoir. This loop is repeated for the same time step until both models converge. Then the next time step is initialized with the last solution and the coupling strategy is repeated for all time steps.

The discretization of the surge pipe-flow model and reservoir model can be seen in Figure 4-2. The discretization of the surge pipe-flow model and reservoir model, where the reservoir reduced to one quarter of its volume due to symmetry and computational concerns.

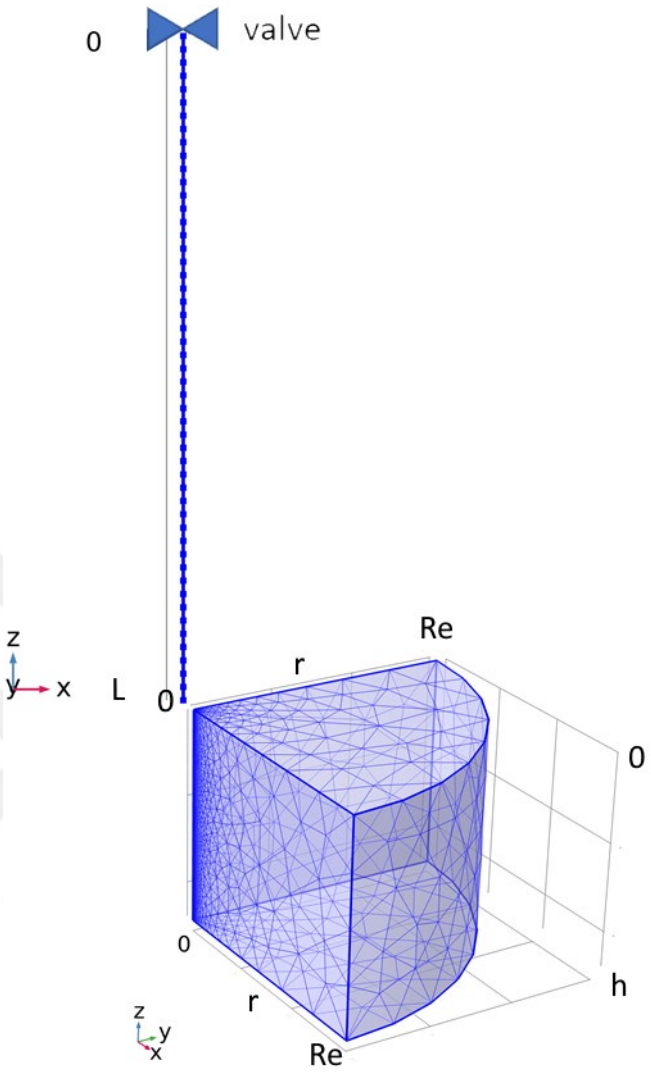

Figure 4-2. The discretization of the surge pipe-flow model and reservoir model

4.4 Possible Field Test Configuration

4.4.1 Downhole Shut-in Tool

Downhole shut-in tools are advanced devices used to close the wellbore at a depth rather than at the surface. This eliminates the influence of wellbore dynamics, leading to faster well pressure stabilization and higher-quality pressure data. These tools often feature precision-engineered valves designed to close instantaneously,

capturing accurate and immediate pressure responses. They are highly durable, typically mounted below locks or plugs, and are built to withstand extreme downhole environments such as high pressure, high temperature, and corrosive conditions.

A pressure recording device, usually positioned below the valve, monitors pressure and temperature changes in the formation during valve operations. The formation is allowed to flow for a specific period to achieve the desired drawdown. After this, the valve shuts in the well, allowing the pressure to stabilize. This process, known as drawdown and build-up testing, can be repeated to gather more data for comprehensive analysis.

Deployment of downhole shut-in tools varies based on operational requirements. They can be lowered into the wellbore attached to tubing strings or via wireline or slickline cables. These tools play a critical role throughout the lifecycle of a well—from drilling and completion to production and intervention activities. Figure 4-3. The schematic of the downhole instand shut-in tool example illustrates a schematic example of a widely used downhole shut-in tool [28], highlighting its design and functionality.

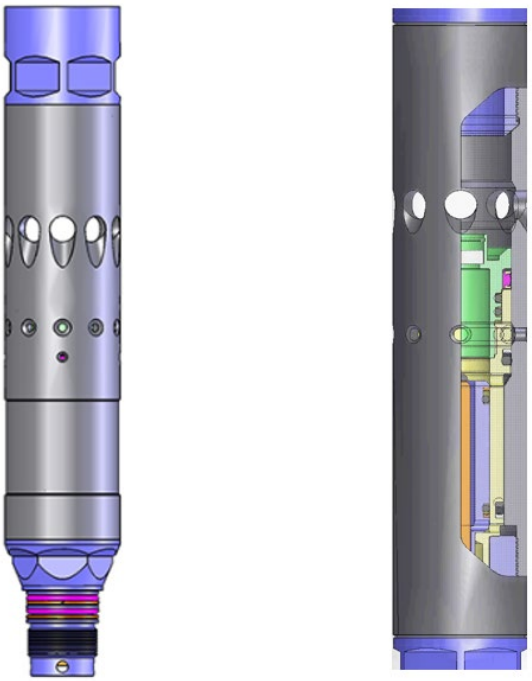

Figure 4-3. The schematic of the downhole instand shut-in tool example

4.4.2 Downhole Pressure Measurement Gauge

Downhole gauges are designed to operate reliably in harsh conditions, including high pressure, high temperature, and corrosive environments. They are essential in oil, gas, and geothermal wells for applications such as pressure build-ups, gradient surveys, well testing, production optimization, and interference testing. These gauges can be deployed using slickline, coiled tubing, drill stems, and other methods tailored to specific operational needs.

For this study, precise and responsive pressure measurement is critical. Compensated crystal quartz gauges are the most widely used in the industry for their exceptional accuracy and reliability [29]. These gauges provide high-quality pressure and temperature data by utilizing a quartz crystal disc placed between two quartz drums. As pressure and temperature change, the disc's natural frequency shifts, enabling precise measurement. These gauges can measure pressures up to 30,000 psi with an

accuracy of ±0.020% and a resolution of 0.00006%, as well as temperatures up to 200 °C with an accuracy of ±0.25 °C and a resolution of 0.005 °C.

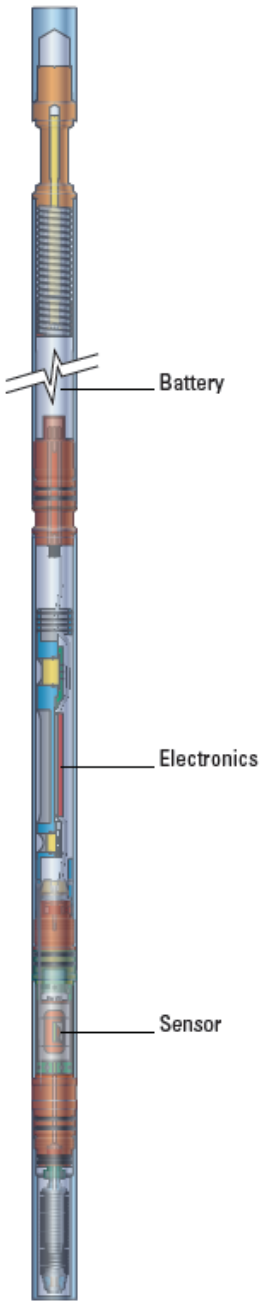

Figure 4-4. Schematic of the downhole quartz gauge assembly and sub components that is commonly used in industry

Quartz gauges are equipped with dual-mode oscillators, which allow dynamic compensation for thermal and transient effects. This ensures rapid stabilization times, making them ideal for detecting small pressure changes over seconds or minutes. Such capabilities are crucial for applications like pressure drawdowns and interference testing. The comprehensive data from quartz gauges provide engineers with clear insights into reservoir boundaries, reserves, and productivity, helping to optimize reservoir management and production strategies. Figure 4-4 presents a schematic of a typical quartz gauge assembly, showing its main components and design considerations.

CHAPTER 5

RESULTS AND DISCUSSION

This chapter is organized in two parts. The first part starts with verification of the newly developed finite-element well–reservoir model against the CLAWPACK-based "pipe + analytical reservoir" framework. We compare simulated pressure data from the down-hole valve location and through the reservoir.

The second part presents a set of sensitivity studies. We run controlled simulations in which one parameter at a time is varied—fluid type and flow rate for oil and gas wells; matrix properties such as permeability and porosity; operational factors like valve-to-reservoir distance; and, for fractured reservoirs, fracture aperture, fracture half-length, and fracture permeability. Each scenario is illustrated with paired plots: valve-head pressure versus time and reservoir pressure versus radius at initial condition and at the end of simulations.

5.1 Testing and Comparison with Finite Element Model

The developed finite element models for the transient pipe and reservoir models by using the finite element is tested and compared with the CLAWPACK-based transient pipe flow model coupled with the analytical reservoir model for verification of the finite element model.

The models are run for a well having proposed test configuration producing from a reservoir with homogenous properties (see Figure 4-1 and Figure 4-2). 500 m length vertical pipe is connected to a reservoir. The parameters of the model are listed in Table 5.1

To create a surge shock, the valve at the well head is starting to close at 0.5 [s] and closes at 0.6 [s] (see Figure 5-1). This abrupt velocity change from initial velocity to

0 velocity within 0.1 seconds creates a shock wave starting at the well head in the well traveling with a speed of 1000 m/s.

Table 5-1 Model parameters

Parameters	Values
Density	700 kg/m³
Dynamic viscosity	6E-4 Pa·s
Speed of sound	1000 m/s
Fluid compressibility	2.18E-9 1/Pa
Porosity	0.25
Permeability	4.93E-14 m²
Friction factor	0.02
Length	500 m
Wipe radius	0.0371 m
Initial flow rate	4.2857E-4 m³/s
Initial velocity in pipe	0.099112 m/s
Radius of reservoir	15.06 m
Thickness of reservoir	12 m
Well radius at sand face	0.1 m
Pressure at well head	1E7 Pa
Courant number	0.1
Number of elements in surge model	50
Outer pressure boundary of the reservoir	1.3801E7 Pa
Output time period	0.05 s
Maximum time step	0.001 s

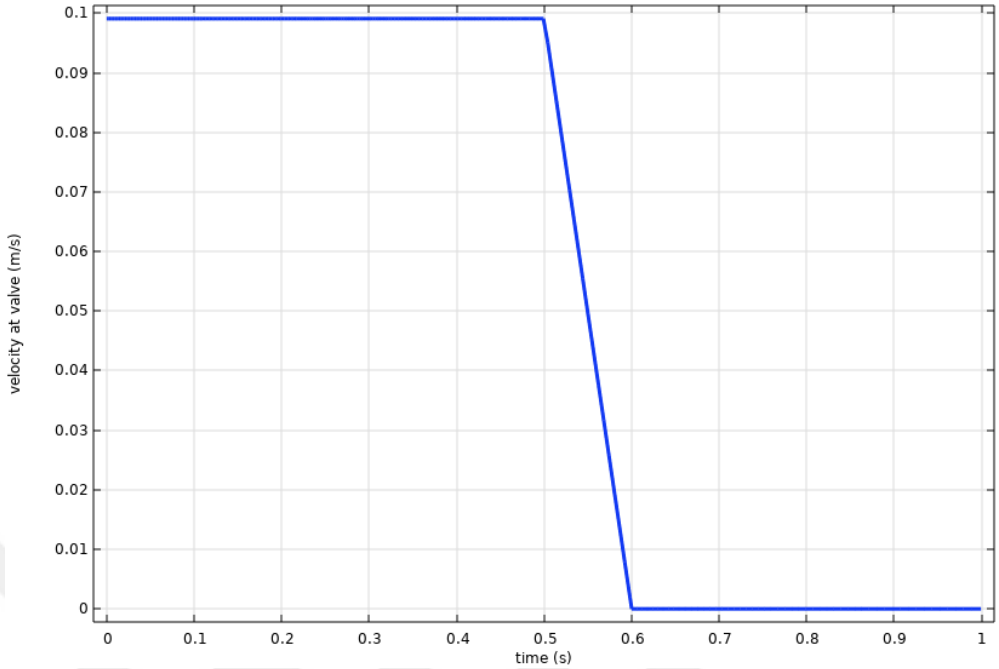

Figure 5-1. Valve closing period: Velocity at valve section vs. time

The pressure surge reaches the reservoir after 0.5 seconds and the pressure at the reservoir sand face starts to increase (see Figure 5-2(a)). The velocity surge is reflected from the reservoir and travels with the speed of sound back and forth within the well, while the velocity at the well head is kept at. The pressure distribution within the reservoir (see Figure 5-2(b)) is also affected by the rate velocity at the reservoir and it is increasing with time.

The pressure distribution within the reservoir is also affected by the pressure and velocity changes at the sandface and it is increasing with time. These trends are observed in both models with almost the same values (see and compares Figure 5-2 and Figure 5-3).

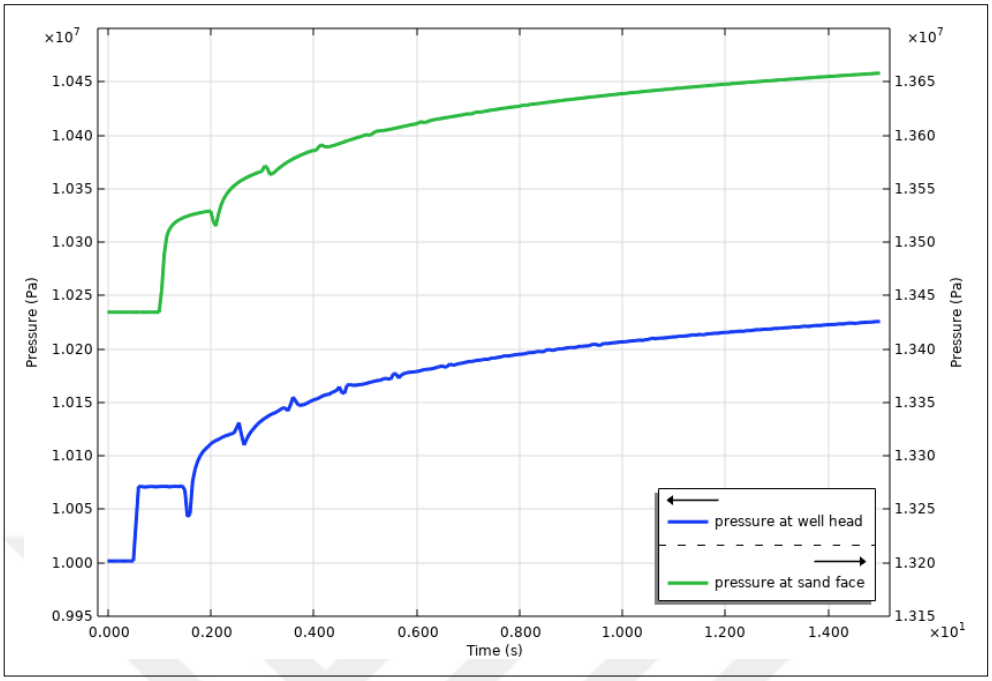

(a)

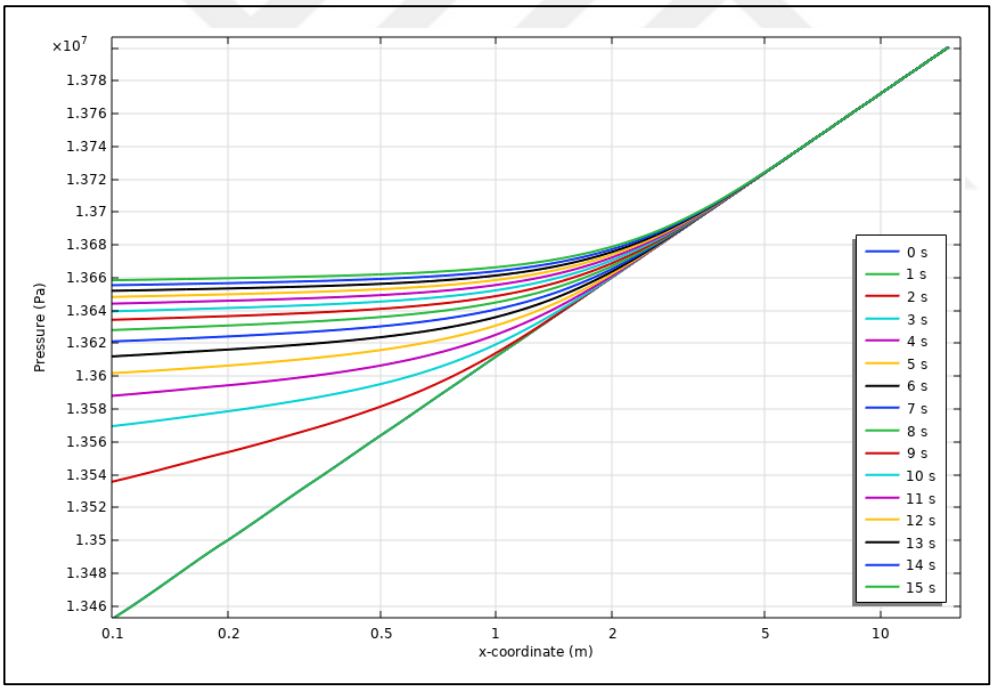

(b)

Figure 5-2. Pressure history at wellhead and bottom hole b) Presure distribution in reservoir obtained by COMSOL models

(a)

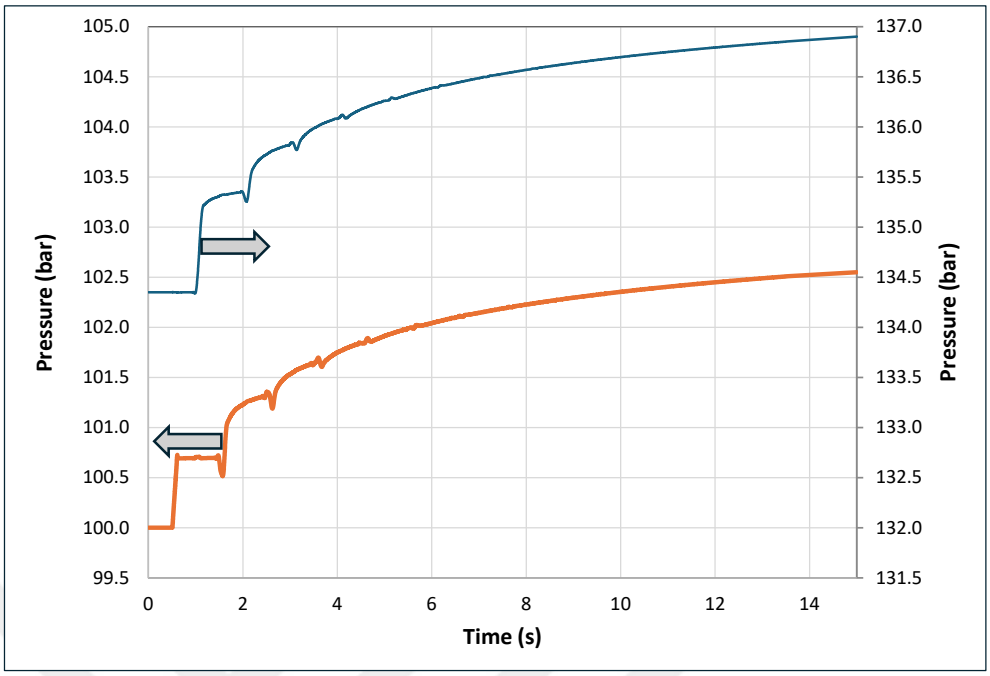

(b)

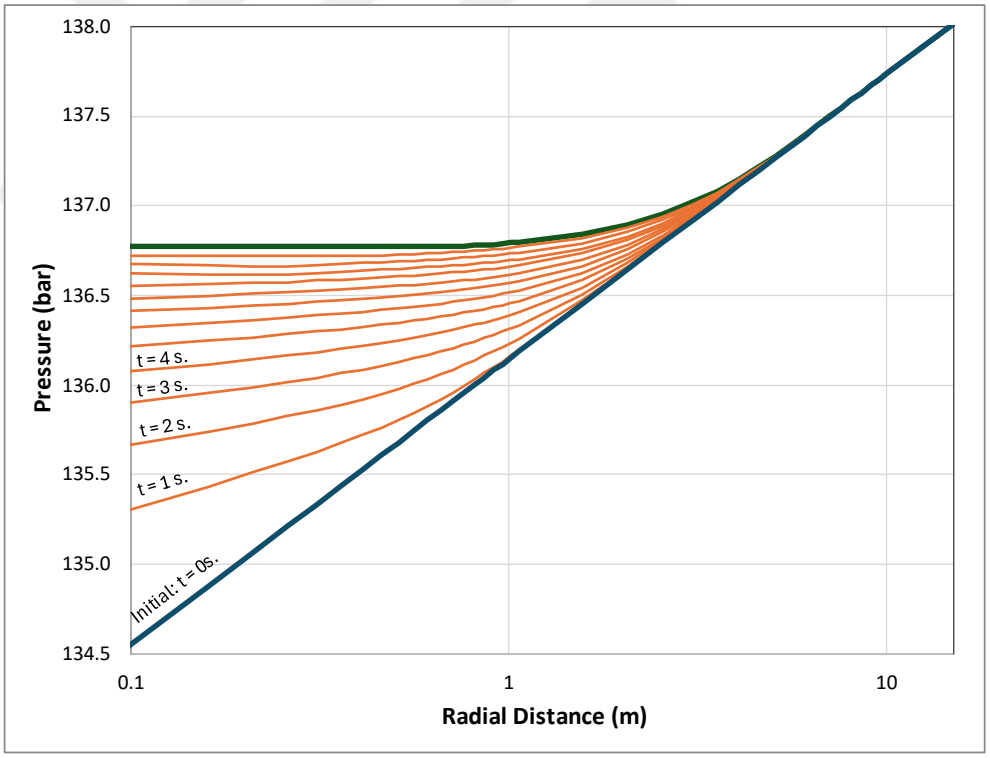

Figure 5-3. a) Pressure history at wellhead and bottom hole b) Presure distribution in reservoir obtained by CLAWPACK-based pipe models and analytical reservoir model

The response of the reservoir to the pressure and velocity surges depends on the properties of the reservoir. In the next sections a parametric sensitivity analysis will be carried out not only by changing reservoir permeability and porosity values but also adding sand face zone, single fracture and multiple fractures to the reservoir.

5.2 Sensitivity Studies

In this section we examine how a sudden valve-closure affects pressure at the valve itself and how that disturbance propagates into the reservoir. To do so, we simulated a series of valve-closure scenarios in which reservoir rock and fluid properties, production rates, and the distance between the valve and the reservoir were varied.

Table 5-2 lists the base-case values together with the alternative values used in the sensitivity analysis. The first group of simulations considers three crude-oil types: light oil (ρ = 800 kg m^{-3}), medium-gravity oil (ρ = 900 kg m^{-3}), and heavy oil (ρ = 970 kg m^{-3}). Because the speed of sound in oil depends on density [30], we used the representative acoustic velocities reported by Wang et al. [30]. rather than employing more complex correlations. Compressibility, likewise related to density and acoustic velocity through C = $1/(\rho c^2)$ was calculated from the same reference.

Table 5-3 lists the parameters of gas reservoir simulation cases. For gas reservoir case model parameters used same and only differences are; (density, speed of sound, compressibility, dynamic viscosity) is calculated by equation of states. Also, gas flow rate used as 30.000, 100.000 and 300.000 Sm3/d.

Additional sensitivity groups covered permeability, porosity, production rate, and the standoff distance between the shut-in valve and the reservoir. When running each group of simulations, all other parameters were held at their default (base-case) values, highlighted in red in Table 5-2 and Table 5-3 for oil and gas reservoir respectively.

Table 5-2 Model parameters for sensitivity analysis in oil reservoir

Parameters	Values and Ranges
Density, ρ, kg/m³	970, 900, 800
Speed of sound, c, m/s	1450 ,1300, 1200
Liquid compressibility, bar^{-1}	$C = 1/(\rho c^2)$
Dynamic viscosity, cp	0.6 cp
Porosity, %	5, 10, 20, 30
Permeability, md	1, 10, 100, 1000
Friction factor	0.02
Length of tubing from valve to reservoir, m	100, 300, 500
Production inner tubing diameter (2 7/8 in)	2.44
Oil flow rate, bbl/day	100, 500, 2500
Thickness of reservoir, m	10
Fracture width, mm	2, 5, 10
Fracture half length, m	5, 10, 20
Open hole well diameter at sand face, m	0.1
Pressure at valve location, bar	200
Valve closing time, s	0.5
Courant number	0.1
Number of elements in surge model	50
Output time period, s	0.05
Maximum time step, s	0.001

Table 5-3 Model parameters for sensitivity analysis in gas reservoir

Parameters	Values and Ranges
Density, ρ, kg/m³	calculated by equation of states
Speed of sound, c, m/s	
Liquid compressibility, bar^{-1}	
Dynamic viscosity, cp	
Porosity, %	5, 10, 20, 30
Permeability, md	1, 10, 100, 1000
Friction factor	0.02
Length of tubing from valve to reservoir, m	100, 300, 500
Production inner tubing diameter (2 7/8 in)	2.44
Gas flow rate, Sm³/day	30000, 100000, 300000
Thickness of reservoir, m	10
Open hole well diameter at sand face, m	0.1
Pressure at valve location, bar	200
Valve closing time, s	0.5
Courant number	0.1
Number of elements in surge model	50
Output time period, s	0.05
Maximum time step, s	0.001

The first case study is sensitivity of oil types (see Figure 5-4). In this case, in all other cases as well, the figure (a) shows transient pressure change at the down-hole valve after sudden closure for three crude-oil densities. The initial water-hammer pressure is related with the product $\rho\, c\, v$ (Joukowsky relation). Hence the heavy crude (ρ = 970 kg m^{-3}, c = 1450 m s^{-1}) produces the largest peak (~3.5×10^5 Pa), the light crude (ρ = 800 kg m^{-3}, c = 1200 m s^{-1}) the smallest (~3.0×10^5 Pa). All three curves show a rapid negative reflection, followed by two or three damped oscillations before merging into a slow logarithmic build-up controlled by reservoir recharge. Because the heavier oil stores more momentum, its oscillations continue slightly longer and the long-term pressure settles ~0.3×10^5 Pa higher than that of the light oil. Peak

amplitude and decay rate are therefore sensitive to fluid density and bulk modulus; neglecting these properties could bias transmissivity estimates derived from valve-pulse data. The figure (b) shows pressure along reservoir at the perforated interval 15 s after valve closure for three oil types. Close to the sand face (x = 0–5 m) heavier oil yields the highest over-pressure because the larger surge at the valve injects more mass into the formation before the wave reflects. Deeper in the reservoir (x > 15 m) the three curves converge, indicating that diffusional smoothing dominates and fluid-property differences become negligible at this time-scale. Practical implication of this cases is that early-time down-hole measurements (first few seconds) are most sensitive to fluid $\rho\, c$; later-time reservoir signatures reflect rock properties almost independently of oil type.

The second analysis is sensitivity to flow rate. As seen in Figure 5-5 the peak surge is proportional to the velocity drop $\Delta v = Q/A$; hence the 2500 bbl d^{-1} case (~1.7×10^{6} Pa) far exceeds the 500 bbl d^{-1} (~3.5×10^{5} Pa) and 100 bbl d^{-1} (~7×10^{4} Pa) tests. Higher-rate wells store more momentum, so their oscillations continues longer and it decays more slowly before merging into the reservoir-controlled build-up. By t=15s the sharp gradients have relaxed, especially for the high-rates, as the surge energy diffuses into the formation. The two lower-rate cases converge much more quickly, indicating limited reservoir disturbance. Another obvious observation is that early-time spatial pressure data are highly sensitive to the rate.

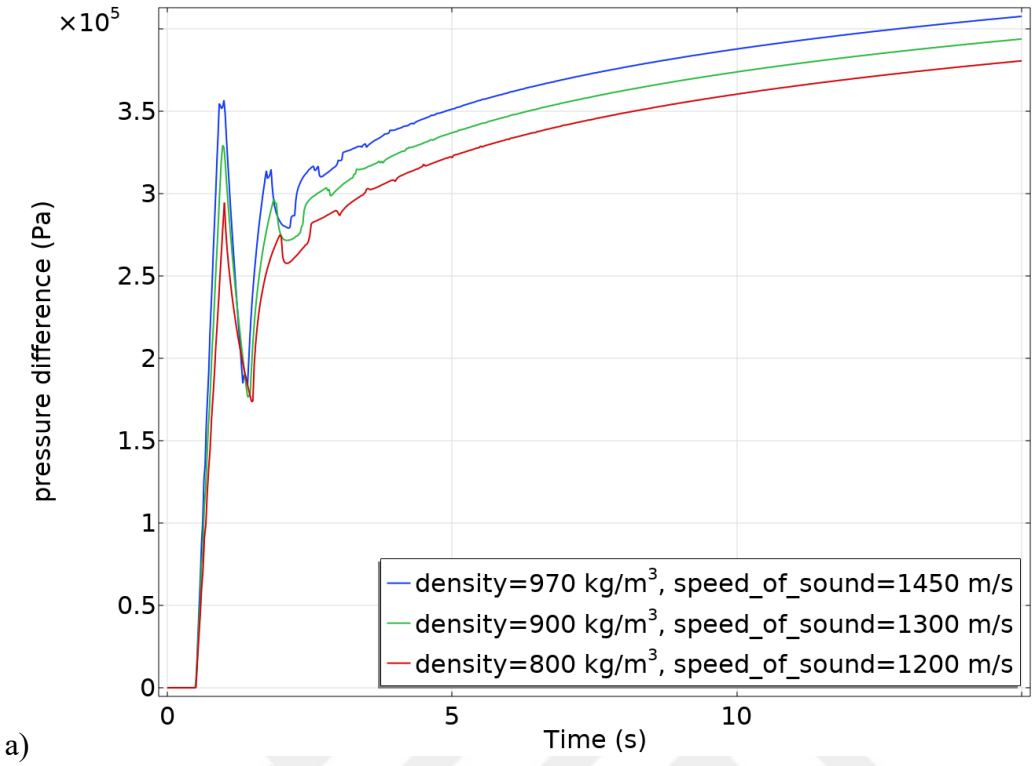

a)

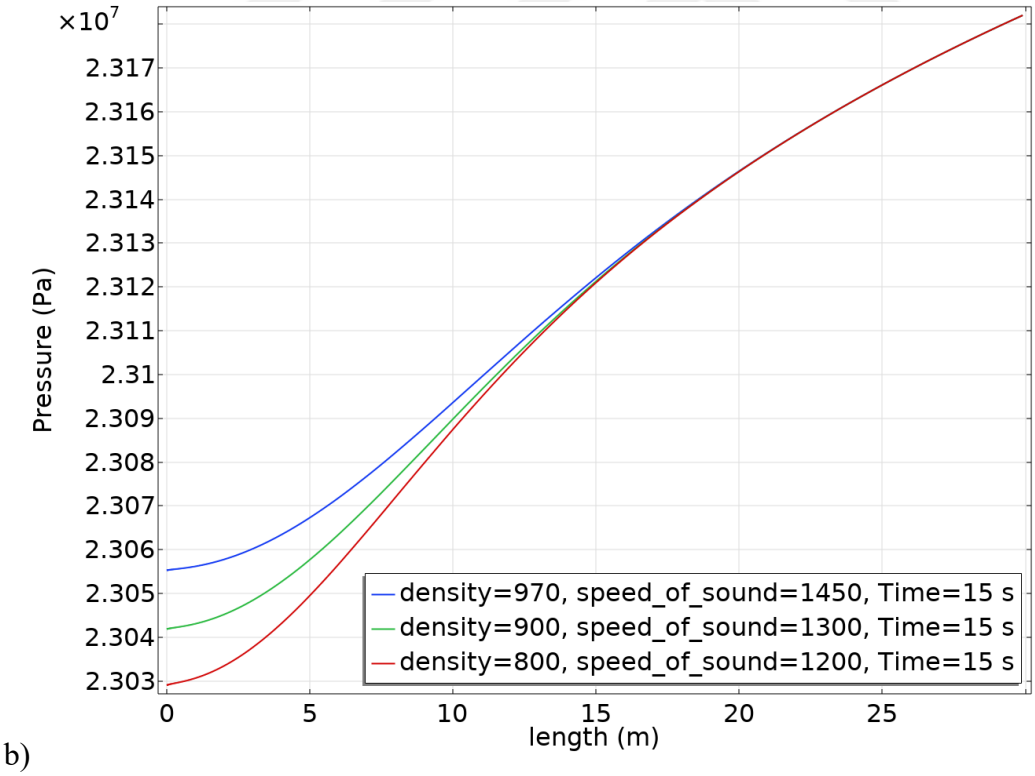

b)

Figure 5-4. Sensitivity results in oil reservoir for oil types: a) Pressure recorded at valve location b) Pressure profile through reservoir

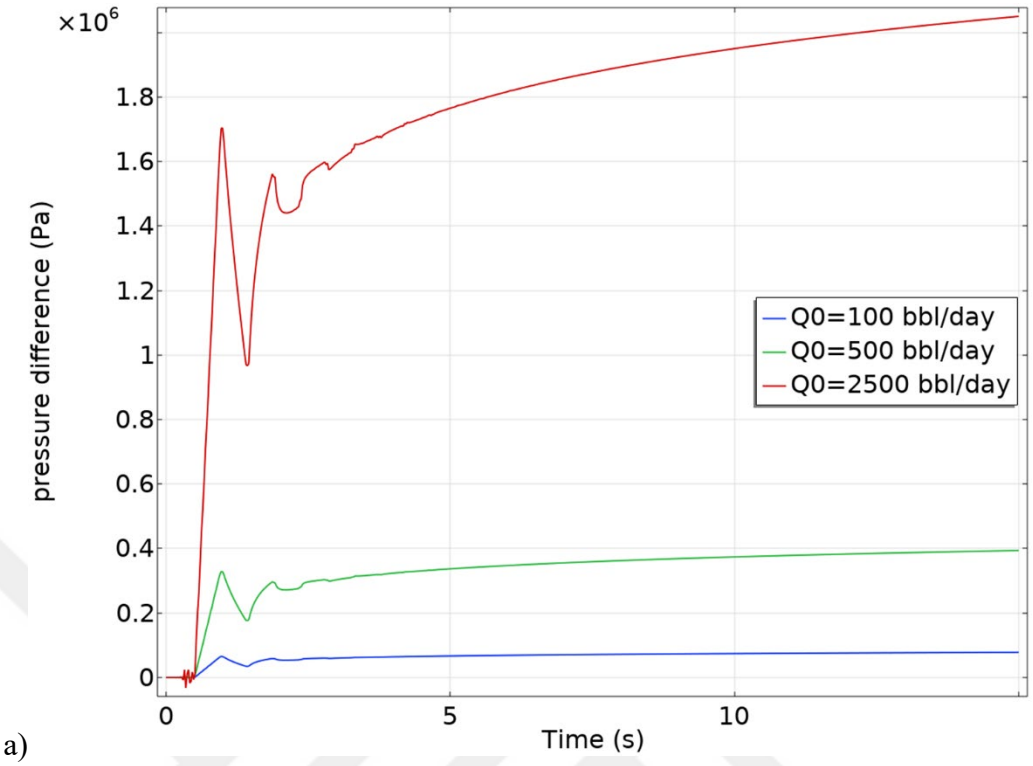

a)

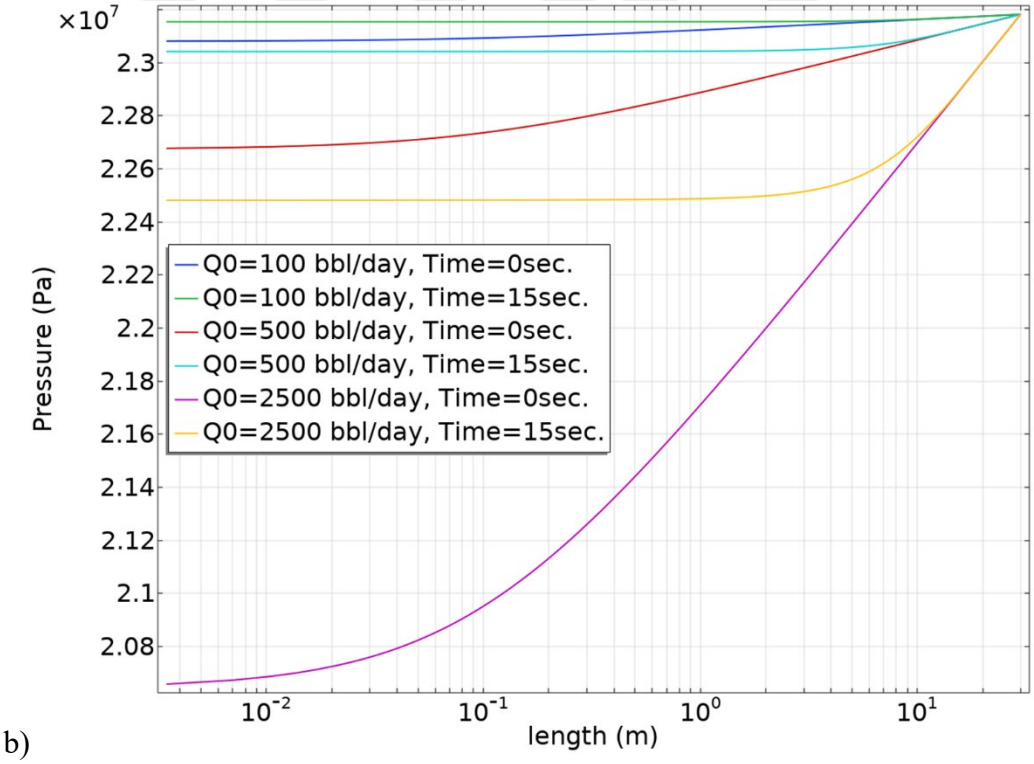

b)

Figure 5-5. Sensitivity results in oil reservoir for oil rate: a) Pressure recorded at valve location b) Pressure profile through reservoir

The third analysis is sensitivity to permeability (Figure 5-6). When permeability is only 1 mD the formation accepts very little fluid, so almost the entire water-hammer pulse is reflected back into the wellbore. The pressure difference increases to ~1×10^7 Pa—two orders of magnitude higher than the 1000 mD case. At 1000 mD the reservoir acts like an open sink: the surge is rapidly absorbed and the pressure difference at the valve never exceeds ~2×10^5 Pa. Oscillations are very small. Low-permeability rock (1 mD) shows a very steep gradient near the wellbore: pressure has risen by ~2.5×10^6 Pa within the first 20 cm. For 1000 mD the gradient is almost flat, confirming that the pulse dissipates quickly into a highly conductive formation. An important observation is that low-k reservoirs show a strong gradient, early pressure-decay data are highly sensitive to transmissivity and can be inverted for k·h. For high permeabilities, the method loses sensitivity; traditional drawdown/buildup tests may be preferable. These results confirm that coupling the water-hammer model with a transient reservoir solver captures the expected inverse relation between permeability and surge amplitude, offering a rapid screening tool for low- to medium-permeability formations.

The fourth analysis is sensitivity to porosity (Figure 5-7). Because porosity does not influence the initial Joukowsky surge (controlled by $\rho\ c\ \Delta v$), all cases have the same water hammer pressure. Low-porosity rock (ϕ = 0.05) stores little fluid, so the pressure difference increases to ~2.05×10^7 Pa and decreases slowly. High-porosity rock (ϕ = 0.30) has four times the storage capacity; the same injected volume produces only ~2.033×10^7 Pa and stabilizes faster. Since storativity is proportional to porosity, higher ϕ quickly absorbs surge energy, lowering the measurable pressure increase. These trends confirm also that the coupled model captures the expected inverse relationship between porosity and water hammer pressure, emphasizing its value for rapid near-wellbore diagnostics.

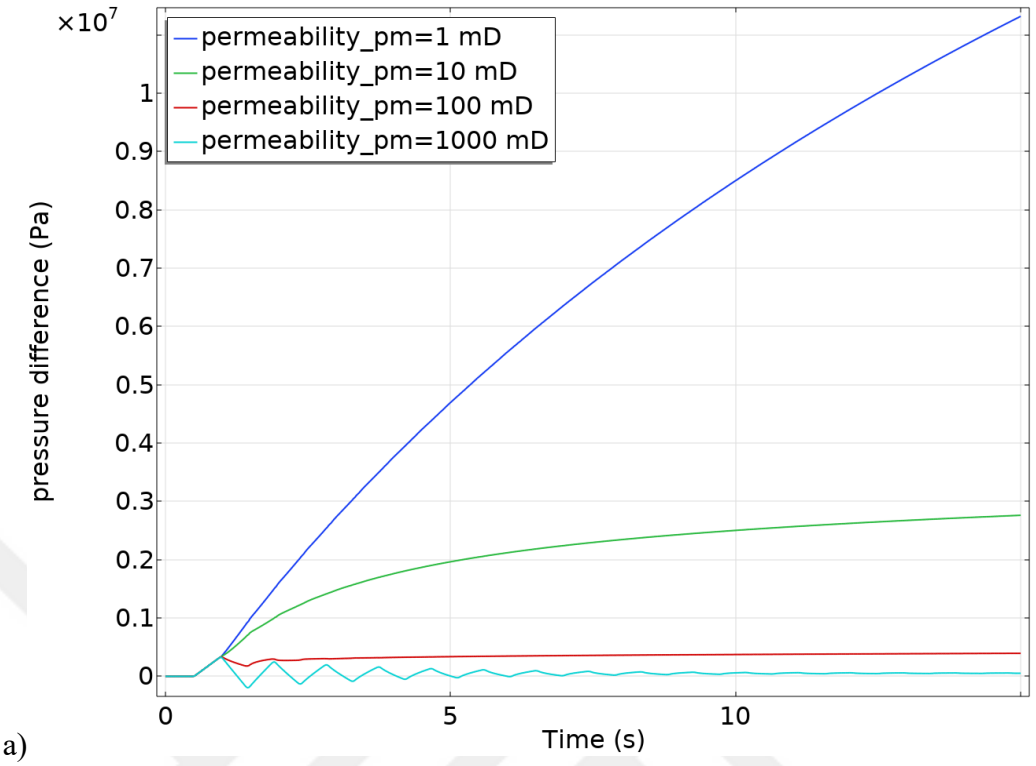

a)

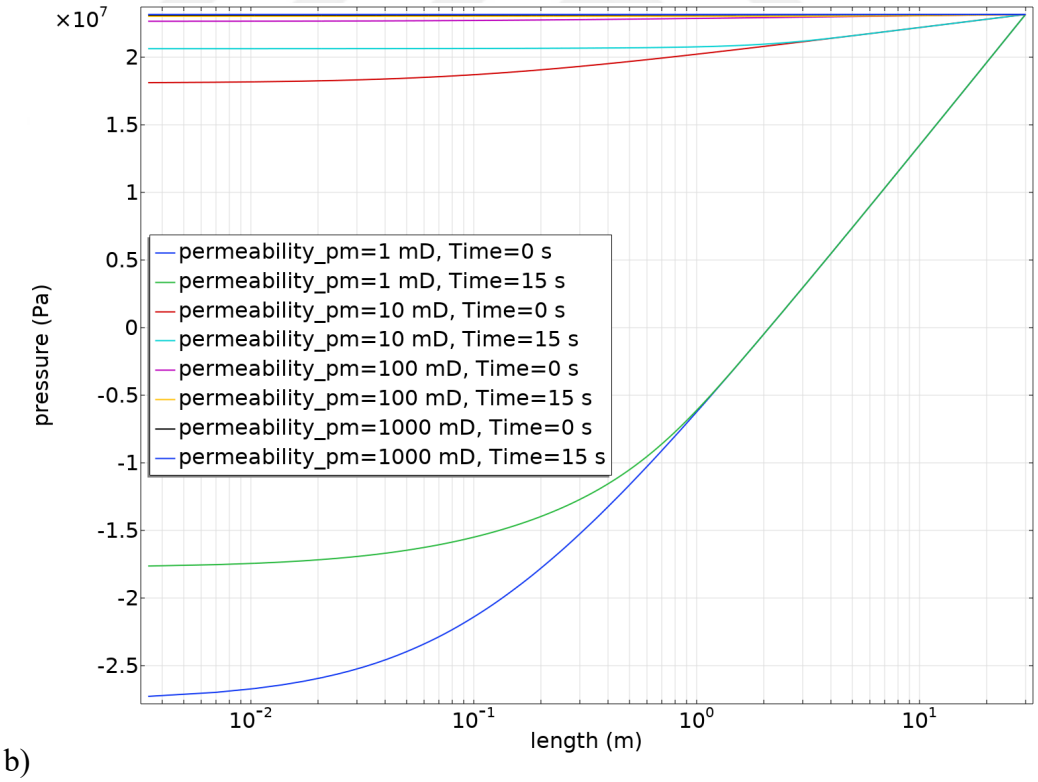

b)

Figure 5-6. Sensitivity results in oil reservoir for permeability: a) Pressure recorded at valve location b) Pressure profile through reservoir

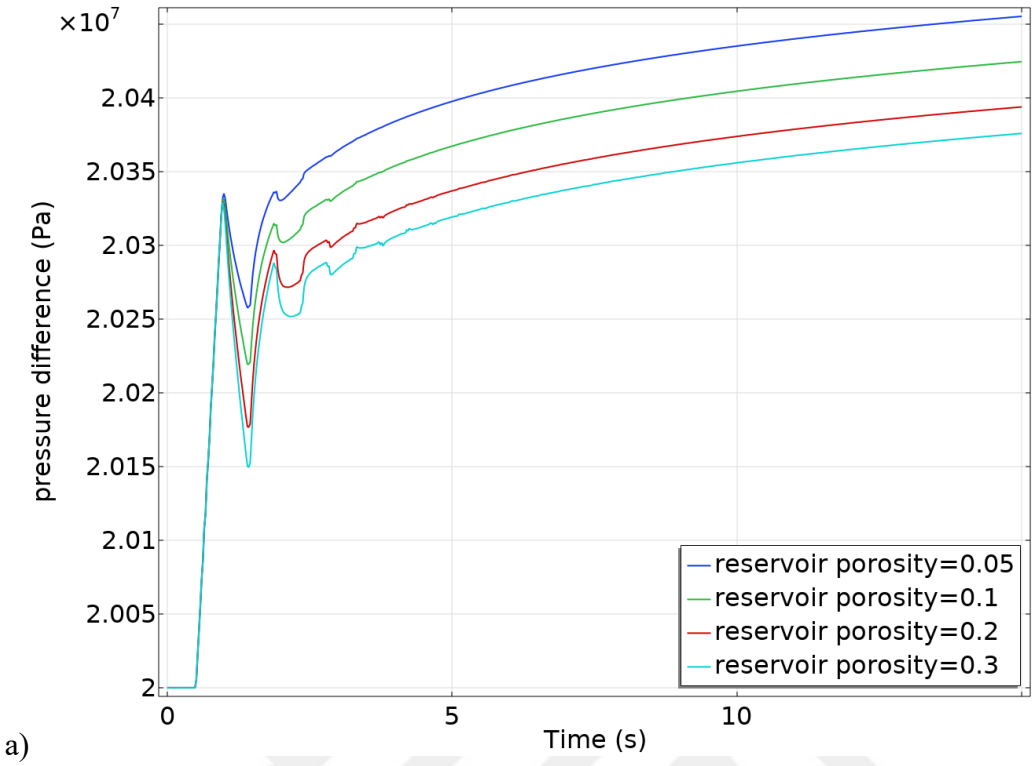

a)

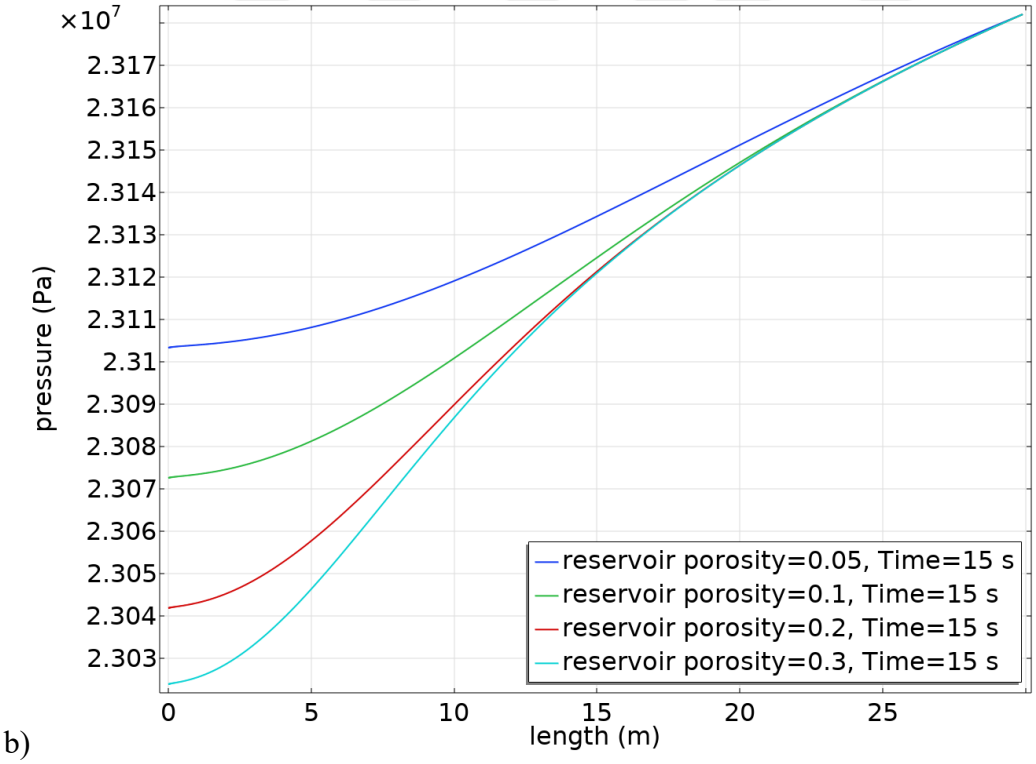

b)

Figure 5-7. Sensitivity results in oil reservoir for porosity: a) Pressure recorded at valve location b) Pressure profile through reservoir

The fifth analysis is sensitivity to valve-reservoir distance (Figure 5-8). The water-hammer pressure is set by $\rho\, c\, \Delta v$ and is therefore independent of pipe length; all three curves start at the same maximum (~3.5×10^5 Pa). If the distance is short, the water hammer pressure wave reflecting back from the reservoir returns to the valve before the valve is completely closed, so some of the energy of pressure wave is lost to downstream of the valve toward to the surface. Since shorter reflection intervals can complicate pulse interpretation, the valve and measurement tools should be located, at least, at the distance of half the value of acoustic velocity × valve closure time (i.e. $x = c \times \Delta t\ /\ 2$) or further away.

The sixth analysis is sensitivity to flow rate in gas reservoir (Figure 5-9). For compressible gas the water-hammer pressure remains proportional to the momentum change as in the case of liquid flow. However, since gas tends to attenuate pressure waves, reflections are weakly damped. As in oil tests, early-time data carry the strongest rate signal; afterwards, formation properties dominate.

The seventh analysis is sensitivity to permeability in gas reservoir (Figure 5-10). For all cases the pressure increases in small, evenly spaced steps. Each step represents the arrival of a reflection from the reservoir after travelling twice the pipe length which might help to estimate acoustic velocity. Low-permeability rock shows the largest cumulative rise because the reservoir can accept only a small fraction of the gas displaced by the water-hammer pulse. As permeability increases, the formation absorbs the surge energy more readily and the pressure increment falls.

The eighth analysis is sensitivity to porosity in gas reservoir (Figure 5-11). The small, equally spaced “steps” that show successive reflections appear at the same times and with the same magnitude for all three cases. In a gas system the surge is dominated by compressibility of the gas itself, so additional pore-volume storage from higher ϕ has only a minor effect on wellbore over-pressure. Unlike the liquid cases, porosity exerts a minimal effect on surge behavior in highly compressible gas systems, and water-hammer tests may not be a practical tool for estimating ϕ in such reservoirs.

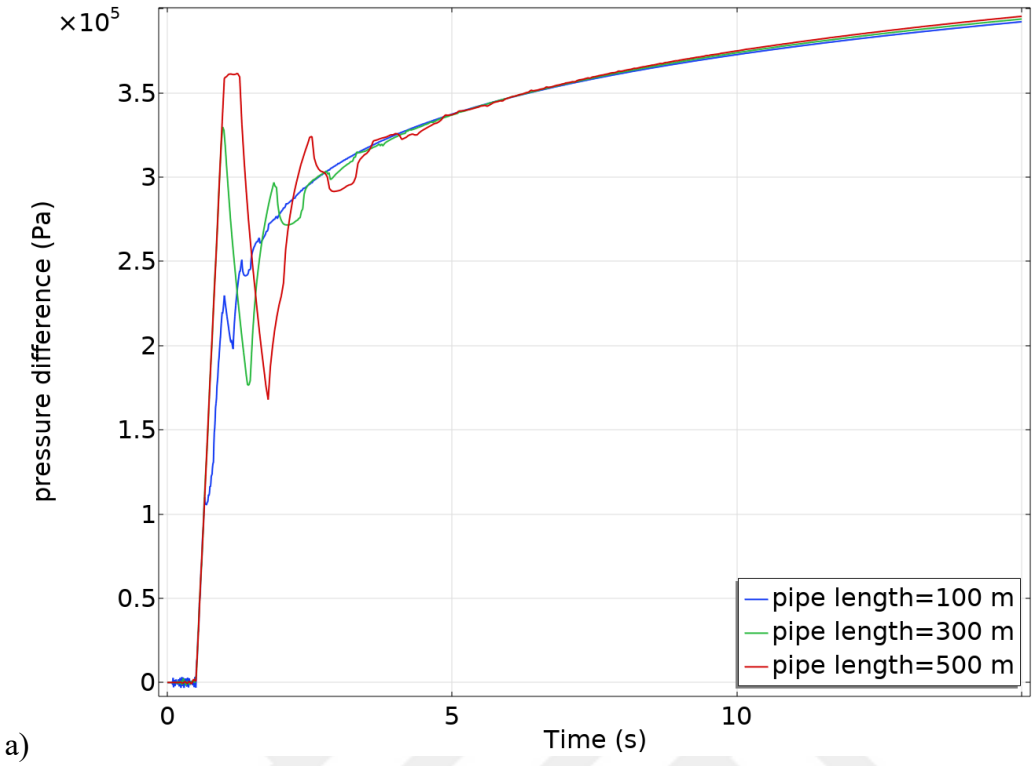

a)

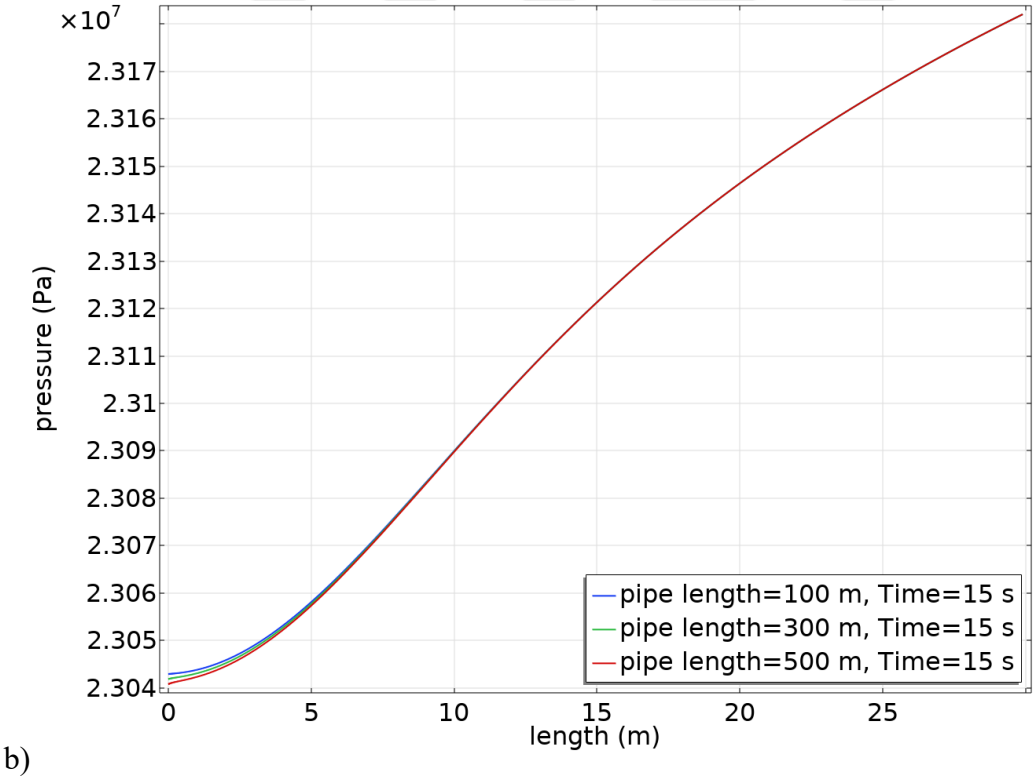

b)

Figure 5-8. Sensitivity results in oil reservoir for tubing length: a) Pressure recorded at valve location b) Pressure profile through reservoir

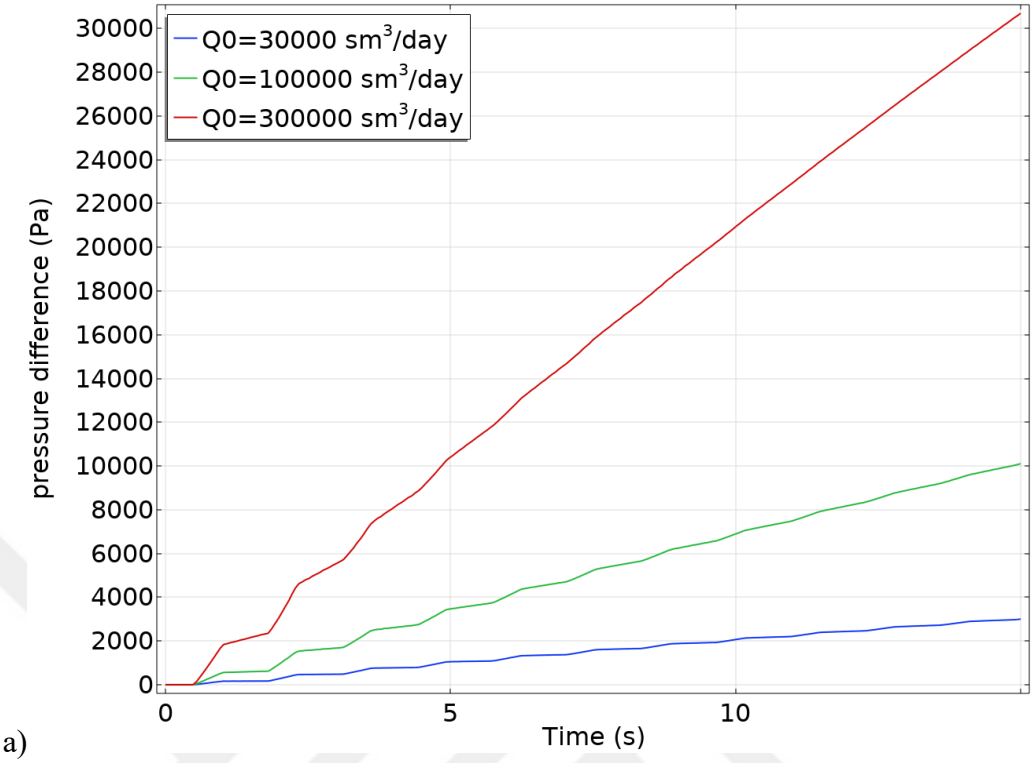

a)

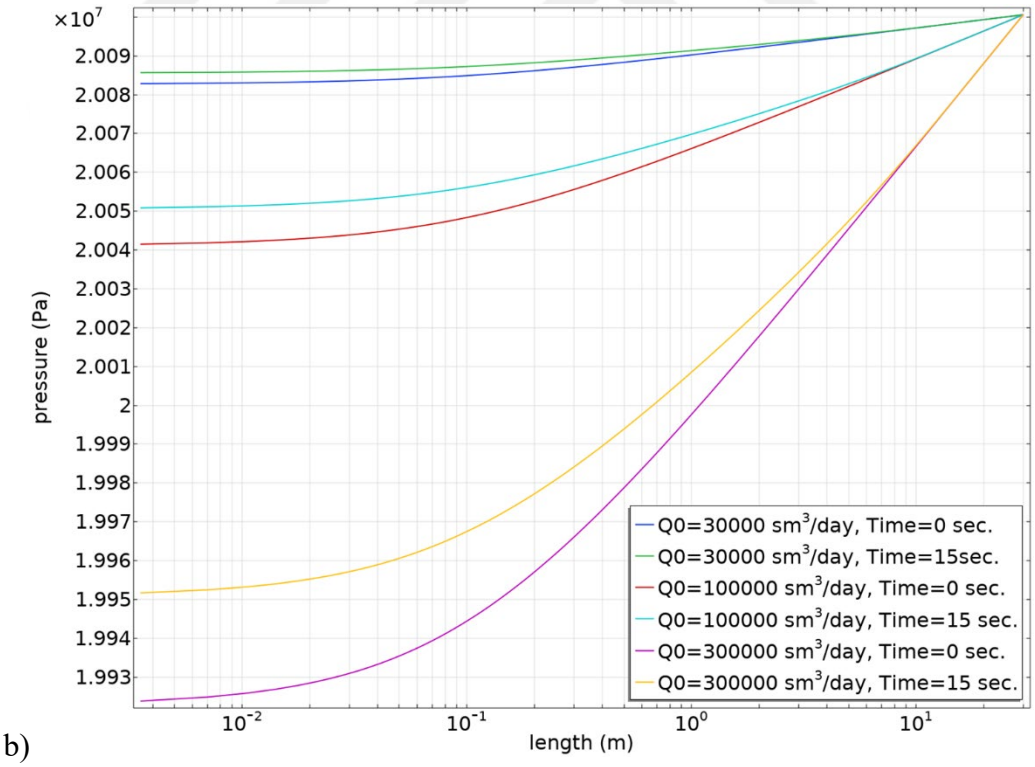

b)

Figure 5-9. Sensitivity results in gas reservoir for rates: a) Pressure recorded at valve location b) Pressure profile through reservoir

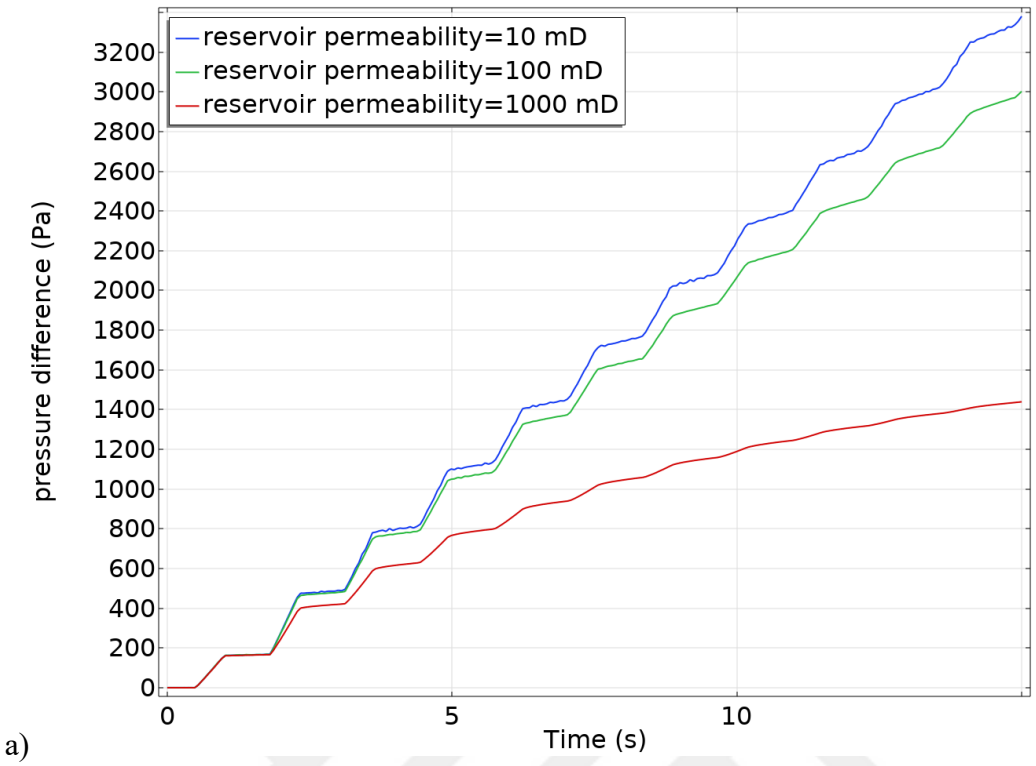

a)

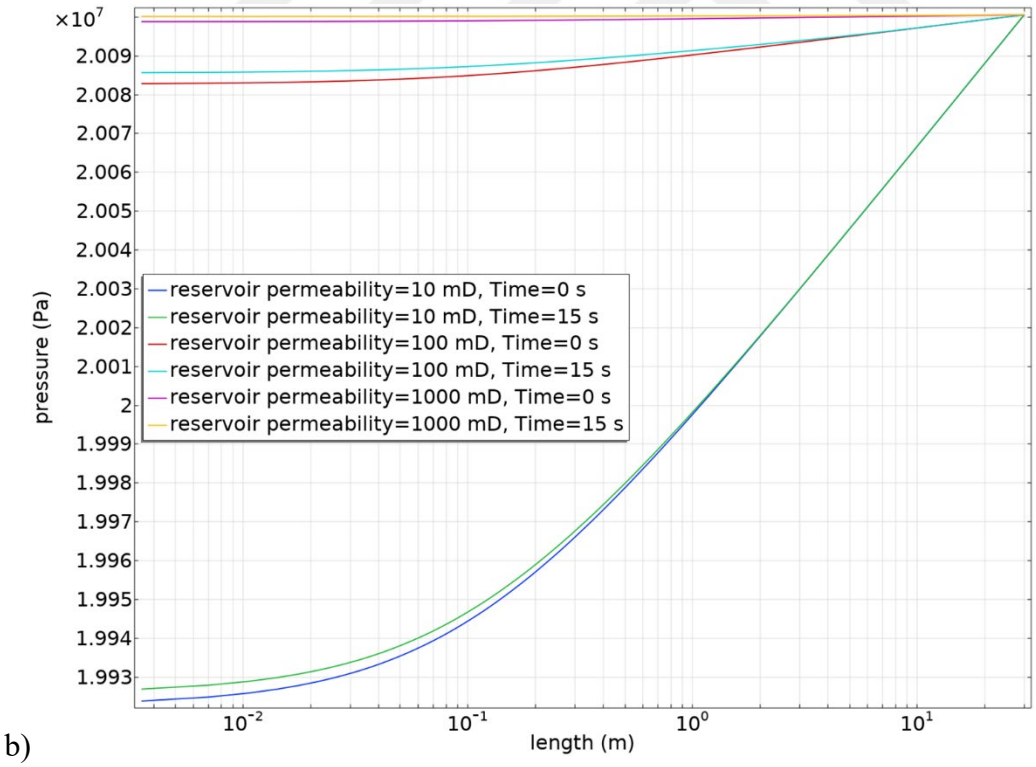

b)

Figure 5-10. Sensitivity results in gas reservoir for permeability: a) Pressure recorded at valve location b) Pressure profile through reservoir

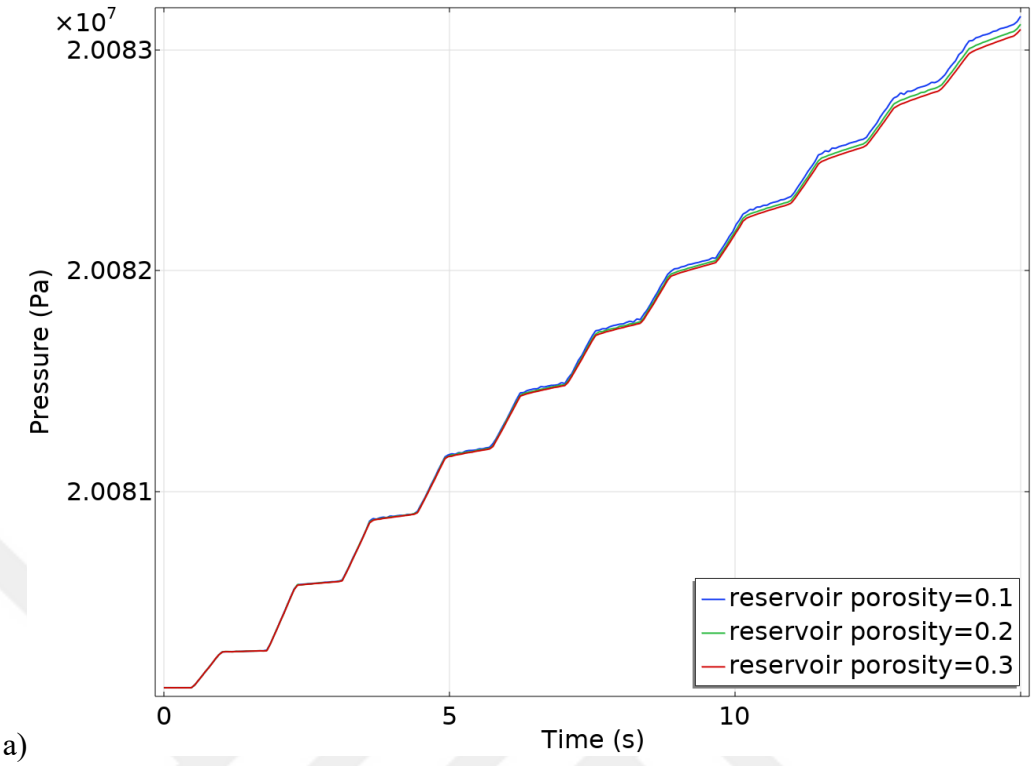

a)

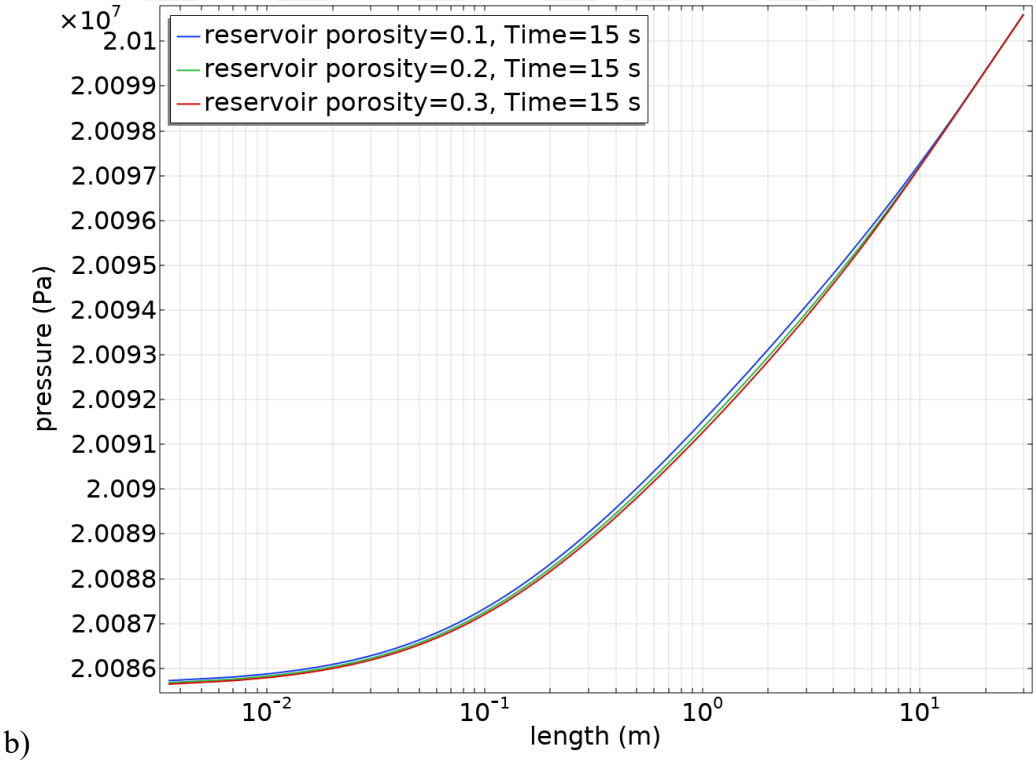

b)

Figure 5-11. Sensitivity results in gas reservoir for porosity: a) Pressure recorded at valve location b) Pressure profile through reservoir

The schematic in Figure 5-12 shows the 3-D numerical domain used for the fractured-reservoir case study. A half-sector of the reservoir volume is retained to exploit symmetry, with the grey surfaces representing the bounding planes. The brown rectangular plane at the center denotes a single, vertical, through-going fracture; its height equals the pay thickness while its half-length extends laterally into the matrix on either side. By embedding the fracture explicitly in this reduced domain, the model captures the coupled flow between fracture and surrounding rock while keeping the mesh size manageable. In the following sensitivity analyses, the fracture attributes—aperture, half-length and fracture permeability—are varied; all matrix properties and outer-boundary conditions remain fixed.

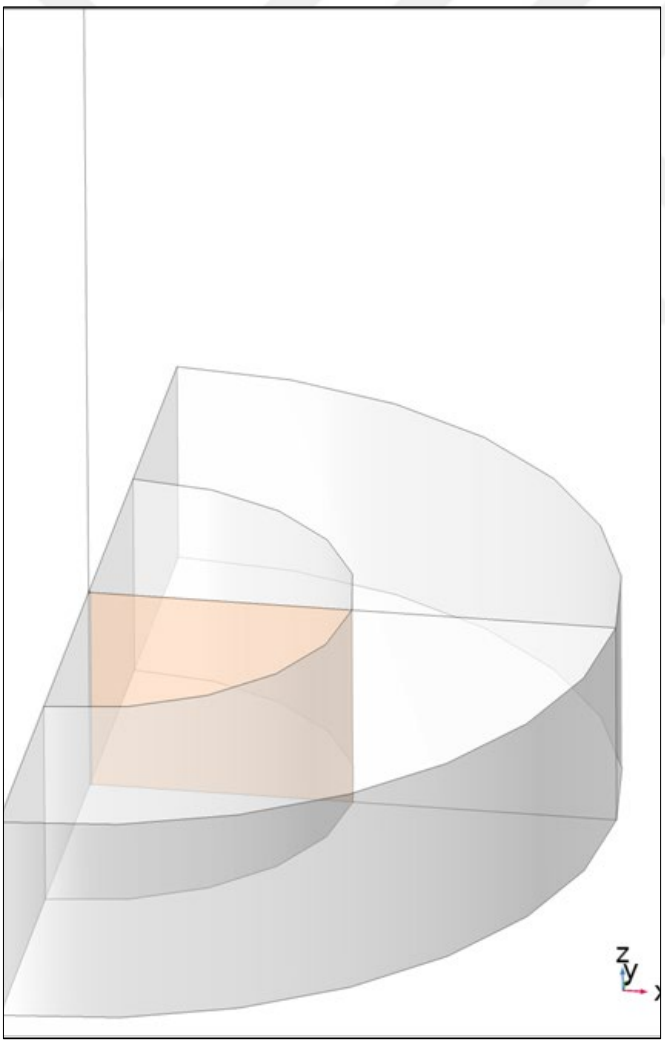

Figure 5-12. Modelled reservoir and fracture schematic

Hydraulic fracture aperture, fracture half-length, fracture permeability plays an important role on evaluating hydraulic fracturing efficiency. Fracture features can be calculated by micro seismic events, or all the pressure data generated by hydraulic fracturing stimulations. However, a sudden change in flow in a confined system results in the formation of a series of pressure pulses known as a water hammer. Pump shutdown or valve closure at the conclusion of a hydraulic fracture treatment frequently generates a water hammer, which sends a pressure pulse down the wellbore that interacts with the created fracture before returning towards the surface. The result is a pressure profile that consists of a series of oscillations that attenuate over time due to friction. The size of this data is much fewer than others so using it to calculate fracture size is efficient.

The goal of this investigation is to simulate the water hammer response of hydraulically fractured wells and quantify how fractures affect the response when the downhole valve shut in few hundred meters above the producing zone.

Accordingly, several sensitivity analysis run using a method of water hammer signal to work out in the modelled fracture reservoir system. The numerical simulation model is proposed based on the transient flow model to describe the water hammer behavior. The impacts of water hammer behavior on fractures are shown from Figure 5-13 to Figure 5-15.

The nineth analysis is sensitivity to fracture aperture in fractured reservoir (Figure 5-13). With a smaller aperture, the fracture shows higher flow resistance, so more of the water-hammer pulse is reflected back into the wellbore and the valve pressure increases to $\approx 1.2\times10^{6}$ Pa. At larger apertures, the fracture acts as an efficient conduit; the surge is partly absorbed and the water hammer pressure reaches only $\approx 1.05\times10^{6}$ Pa. The pressure drop inside the fracture is steeper for the narrow aperture, reflecting its higher hydraulic resistance. Wider apertures show a lower gradient. Once the flow enters the matrix the three curves merge, confirming that aperture influences only the fracture-dominated zone and has insignificant impact on the far-field pressure front at this time scale.

The tenth analysis is sensitivity to fracture half-length in fractured reservoir (Figure 5-14). Shorter fractures yield the largest valve pressure difference (~1.18×10^6 Pa at 15 s). Flow must travel a shorter, higher-resistance path into the matrix, so more of the water-hammer energy is reflected back into the well. When the half-length increases, the fracture presents a larger contact area with the matrix, relieving the surge more efficiently; the valve pressure plateaus near 1.05×10^6 Pa. Past the fracture tip, shorter fracture shows the steepest matrix gradient, whereas longer fracture already approaches the far-field pressure, this reveals that a longer fracture transmits the surge deeper into the reservoir.

The eleventh analysis is sensitivity to fracture permeability in fractured reservoir (Figure 5-15). When fracture permeability is low, the fracture presents greater flow resistance, so a larger share of the water-hammer pulse is reflected into the wellbore; the valve pressure increases to $\approx1.28\times10^6$ Pa at 15 s. At higher fracture permeability, the fracture behaves almost like an open conduit. The surge is absorbed more readily and the pressure increase stabilizes near 1.03×10^6 Pa. Past ~10 m the three profiles merge, confirming that fracture permeability only governs pressure loss inside the fracture; once flow enters the matrix, rock properties dominate.

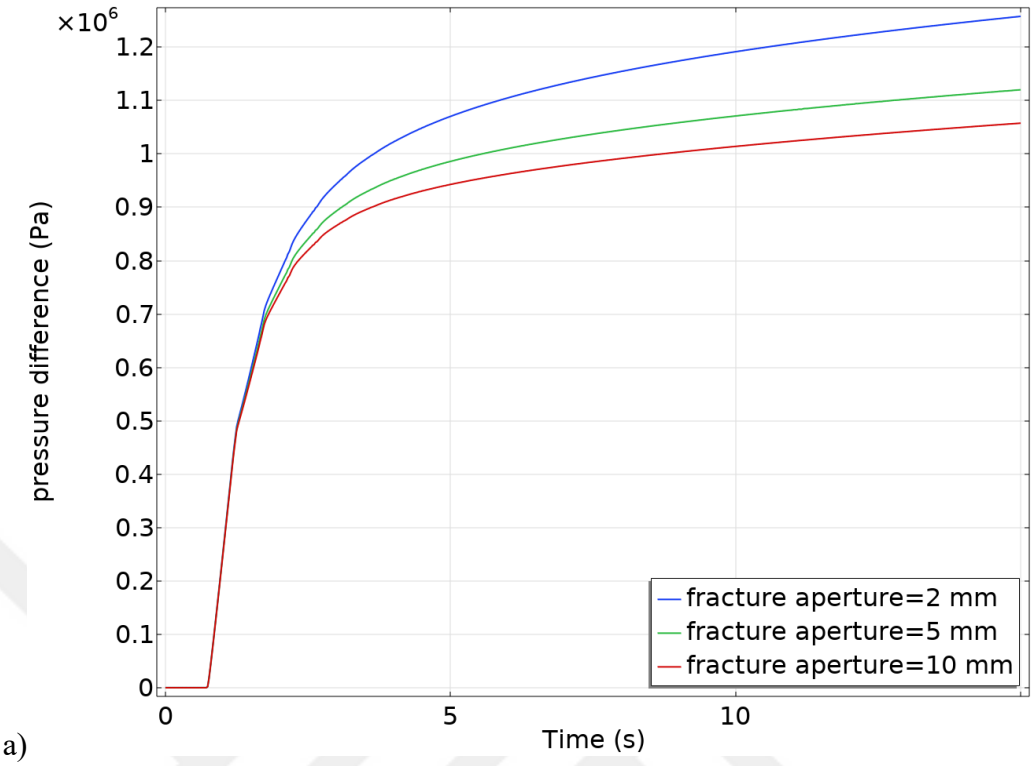

a)

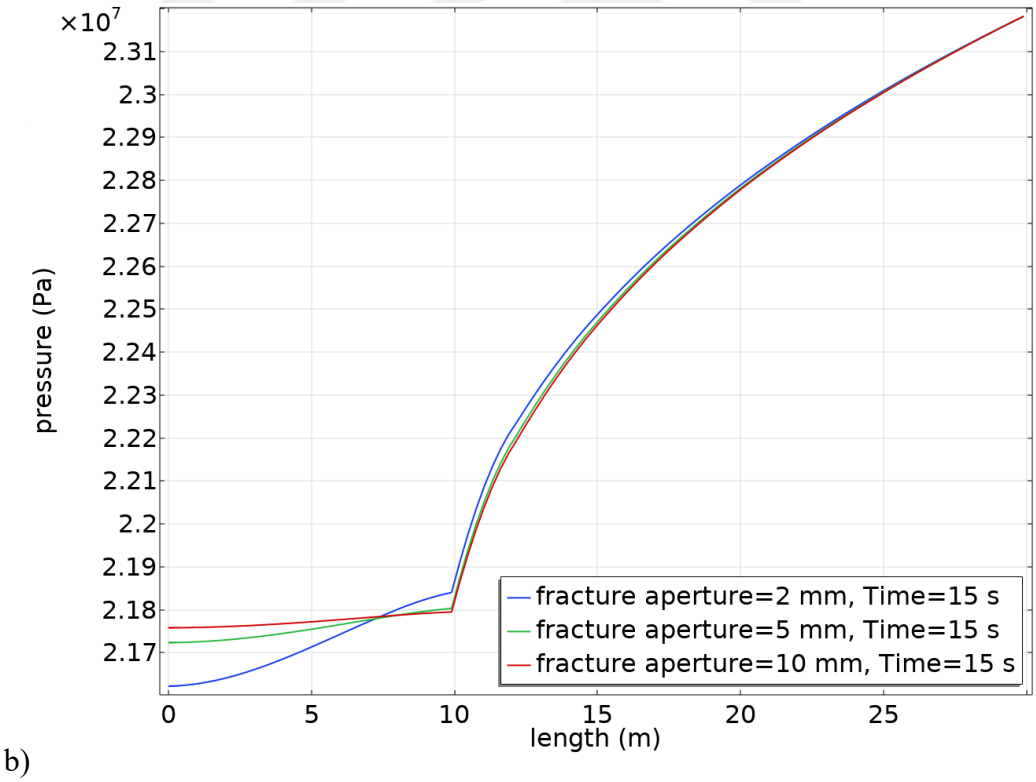

b)

Figure 5-13. Sensitivity results in fractured oil reservoir for fracture aperture:

a) Pressure recorded at valve location b) Pressure profile through reservoir

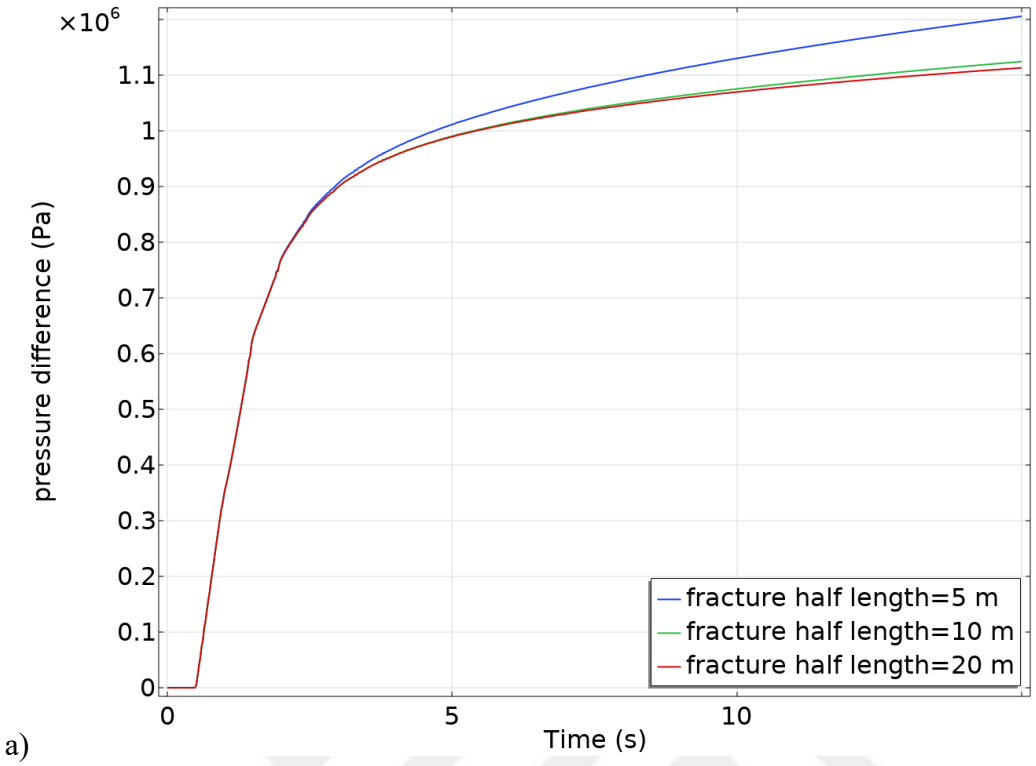

a)

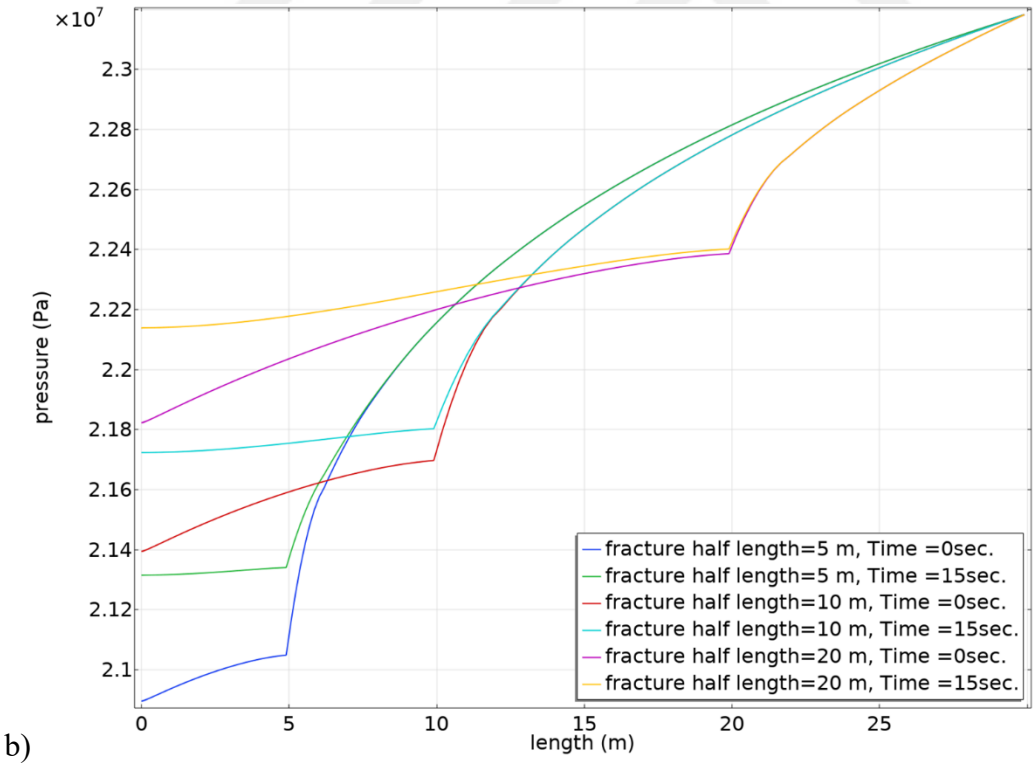

b)

Figure 5-14. Sensitivity results in fractured oil reservoir for fracture half length:

a) Pressure recorded at valve location b) Pressure profile through reservoir

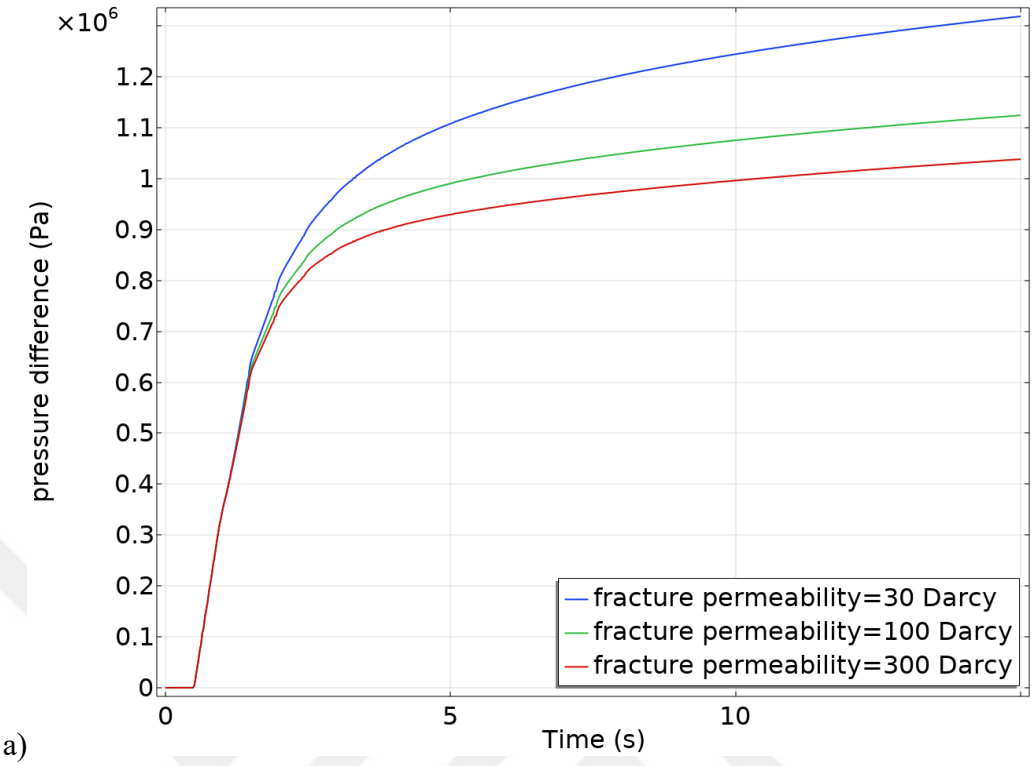

a)

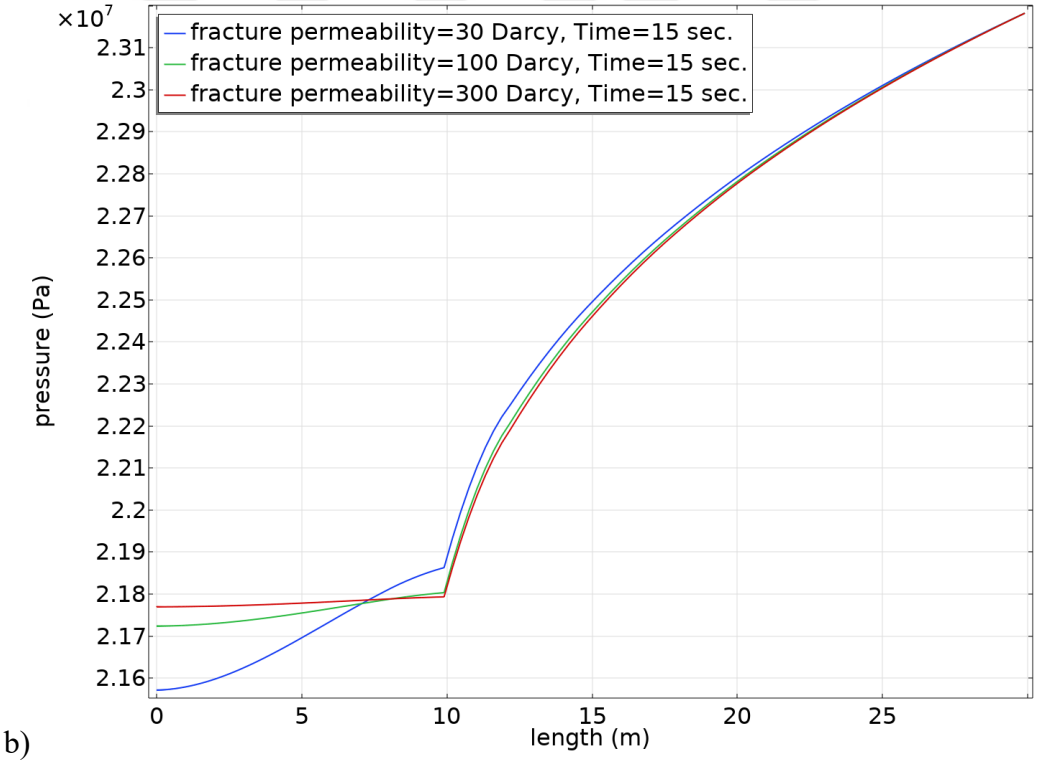

b)

Figure 5-15. Sensitivity results in fractured oil reservoir for fracture permeability: a) Pressure recorded at valve location b) Pressure profile through reservoir

CHAPTER 6

CONCLUSION

This thesis demonstrates that down-hole water-hammer tests, interpreted with coupled wellbore-reservoir models, can provide rapid estimates of near-wellbore properties. We first validated a lightweight hybrid framework consisting of a one-dimensional hyperbolic pipe-flow solver linked to the analytical line-source solution of the diffusivity equation. This model reproduced measured valve-head pulses in single-phase oil wells and served as a benchmark for extensive sensitivity studies.

To capture heterogeneity, fracture flow and pressure-dependent rock/fluid properties, we then built a fully three-dimensional finite-element model. The extended scheme simultaneously resolves transient tubing hydraulics and porous-medium flow, allowing explicit representation of fractures. Comparative simulations show that placing the fast-acting valve and quartz gauge down-hole increases signal amplitude by an order of magnitude and shortens interpretation time to a few seconds.

Key findings from the sensitivity analysis include:

- Surge amplitude scales with $\rho\ c\ \Delta v$ and is therefore largest for heavy oils and high flow rates.
- Valve-head pressure increase is inversely proportional to matrix permeability, providing a quick permeability indicator.
- In fractured reservoirs, aperture controls the early-time pulse, while half-length governs how far the disturbance penetrates; fracture permeability mainly affects pressure loss inside the fracture.
- Porosity has a strong effect in oil systems but is almost negligible in gas reservoirs due to high gas compressibility.

These insights confirm the method's capability to distinguish important variations in both wellbore and reservoir conditions and underline its potential as a diagnostic tool.

Future work will focus on several key advancements to enhance the applicability and robustness of the proposed model.

First, the model will be extended to fully multiphase flow conditions to account for the complex interactions between gas, oil, and water phases in pipe flow and in heterogeneous reservoirs. This enhancement will allow for a more accurate representation of real reservoir behavior.

Second, the workflow will incorporate automated history-matching algorithms to enable real-time parameter estimation. This integration will improve the efficiency and accuracy of model calibration by minimizing manual intervention and leveraging advanced optimization techniques.

Finally, the developed workflow will be applied and validated using field data including sandstone, limestone, hydraulicly or naturally fractured reservoirs, tight-gas formations etc. This application aims to refine the characterization of different formation types and enhance the predictive capabilities of the model under complex geological settings. These future developments will collectively contribute to a more comprehensive and field-ready solution for dynamic reservoir characterization and management.

REFERENCES

[1] Joukowsky, N., Über den hydraulischen Stoss in Wasserleitungsröhren, (On the hydraulic hammer in water supply pipes.) Mémoires de l'Académie Impériale des Sciences de St.-Pétersbourg (1900) Series 8, 9(5), 1-71 (in German)

[2] Frizell, J.P., Pressures resulting from changes of velocity of water in pipes, Transactions of the ASCE. 1898, Vol. 39, pp. Paper 819, 1-18.

[3] Allievi, L., Teoria generale del moto perturbato dell'acqua nei tubi in pressione (colpo d'ariete). (General theory of the variable motion of water in pressure conduits.). Annali della Società degli Ingegneri ed Architetti Italiani. 1902, pp. 17(5), 285-32.

[4] Kries, J., Studien zur Pulslehre, Freiburg im Breisgau and Tübingen, Germany, Akademische Verlagsbuchhandlung von J. C. B. Mohr (Paul Siebeck), 1892.

[5] Ghidaoui, M. S., Zhao, M., McInnis D. A., Axworthy, D. H., A Review of Water Hammer Theory and Practice, Applied Mechanics Reviews. 2005, Vols. 58(1), 49-76.

[6] Krehl, P.O., History of Shock Waves, Explosions and Impact: A Chronological and Biographical Reference. Springer Science & Business Media, 2008.

[7] Wylie, E.B. and Streeter, V.L. Fluid Transients in Systems. New Jersey : Prentice-Hall, 1993.

[8] Messahel, R., Cohen, B., Souli, M., Moatammedi, M., Fluid-structure interaction for water hammers effects in petroleum and nuclear plants. Journal of Fluid Mechanics. 2015, Vols. 12(3), 299-312.

[9] Han, G., Ling, K., Khor, S. H., Zhang, H., Thakur, R. K., Simulation of Multiphase Fluid-Hammer Effects During Well Startup and Shut-in, Paper SPE 160049, presented at the SPE Asia Pacific Oil and Gas Conference and Exhibition, Perth, Australia, 22–24 October 2012 :

[10] Wan, W., Zhou, Y., Geng, C., He, B., Numerical modeling of cavity collapse water hammer in pipeline systems: Internal mechanisms and influential factors of transient flow and secondary pressure rise dynamics. Physics of Fluids. 2023, Vols. 36(8), 087167.

[11] Santarelli, F.J., Skomedal, E., Markestad, P., Berge, H.I., Nasvig, H., Sand Production on Water Injectors: Just How Bad Can It Get? . SPE Drill. & Compl. 2000, Vol. 15(2): 132.

[12] Vaziri, H., Nouri, A., Hovem, K., Wang, Computation of Sand Production in Water Injectors, Paper SPE 107695 presented at the European Formation Damage Conference, Scheveningen, The Nederland, 30 May-1 June 2007.

[13] Wang, X., Hovem, K., Water Hammer Effects on Water Injection Well Performance and Longevity. Paper SPE 112282 presented at the SPE International Symposium and Exhibition on Formation Damage Control, Lafayette, Lousina, USA, 13-15 February 2008.

[14] Livescu, S., Watkins, T. J., Water Hammer Modeling in Extended Reach Wells. Paper SPE 168297 presented SPE/ICoTA Coiled Tubing & Well Intervention Conference and Exhibition, The Woodlands, TX, USA, 25-26 March 2014.

[15] LeVeque, R. J., Finite Volume Methods for Hyperbolic Problems, Cambridge: Cambridge University Press, 2002.

[16] Clawpack Development Team, Clawpack (Conservation Laws Package), 2015. [Online]. Available: http://www.clawpack.org.

[17] Bale, D. S., LeVeque, R. J., Mitran, S., Rossmanith, J. A., A wave propagation method for conservation laws and balance laws with spatially varying flux functions, SIAM Journal on Scientific Computing, vol. 24(3), pp. 955-978, 2002.

[18] Gudmundsson, J. S., Celius, H. K., Gas-Liquid Metering Using Pressure-Pulse Technology, SPE Paper 56584, Presented at the Annual Technical Conference and Exhibiton, Houston, TX, USA, 3-6 October 1999.

[19] Gudmundsson, J. S., Durgut, I., Celius, H. K., Korsan, K., Detection and Monitoring of Deposits in Multiphase Flow Pipelines Using Pressure Pulse Technology, Presented at the 12th International Oil Field Chemistry Symposium, Geilo, Norway, 1-4 April 2001.

[20] Torres, L. , Besancon, G., Georges, D. Mexico, A collocation model for water-hammer dynamics with application to leak detection, 2008. 47th IEEE Conference on Decision and Control, Cancun, pp. 3890-3894.

[21] Ayed, L., Hadj-Taieb, L., Water hammer wave for leak detection in elastic and viscoelastic pipes. International Journal of Mechanics and Energy. 2013, Vols. Vol. 1, Issue 4, pp. 164-171.

[22] Horne, R., Modern Well Test Analysis, A Computer Aided Approach, Petroway, 2nd edition, 1995.

[23] Archer, R., Yıldız, T.T., Transient Well Index for Numerical Well Test Analysis, Paper SPE 71572, Presented at the SPE Annual Technical Conference and Exhibition, New Orleans, Louisiana, USA, October 2001.

[24] Carey, M. A., Mondal, S., Sharma, M. M., Analysis of Water Hammer Signatures for Fracture Diagnostics, Paper SPE 174866, Presented at the SPE Annual Technical Conference and Exhibition, Houston, Texas, USA, 28–30 September 2015.

[25] Durgut, I, Gudmundsson, J.S., Di Lullo, A., Investigating Use of Pressure Pulses To Assess Near Wellbore Reservoir Parameters. Selcuk Univ. J. Eng. Sci. Tech. 2019, Vols. v.7, n.2, pp. 331-345.

[26] Adiputro, A. S., Zarrouk, S. J., Clarke, R. J., Harcouët-Menou, V., and Bosc, S., Geothermal wells with water hammer during injection fall-off test:

Numerical pressure transient analysis, Geothermics, Vols. vol. 87, Art. no. 101838, Apr. 2020.

[27] Deng, S., Yi, L., Li, X., Yang, Z. and Zhang, N., A diagnostic model for hydraulic fracture in naturally fractured reservoir utilising water-hammer signal, Engineering Fracture Mechanics, Vols. Vol. 325, Art. no. 111347, 2025.

[28] Leutert, Quick Shut-In Tools, Leutert, 2025. [Online]. Available: https://www.leutert.com/media/oilgas/downloads/gauges/tools/ShutIn-Tool-Production-Valve-3.5.pdf. [Accessed 2025].

[29] SLB, Signature CQG Crystal Quartz Gauge, 2025. [Online]. Available: https://www.slb.com/-/media/files/testing-services/product-sheet/signature-cqg-gauge-ps-2.pdf. [Accessed 2025].

[30] Wang, Z., Nur, A. M., and Batzle, M. L., Acoustic velocities in petroleum oils, Journal of Petroleum Technology, vol. 42(2) , p. 192–200, Feb. 1990.

CURRICULUM VITAE

Surname, Name: Yildiz, Tabiat Tan

EDUCATION

Degree	Institution	Year of Graduation
MS	TAMU, Petroleum Engineering	2001
BS	ITU, Petroleum and Natural Gas Engineering	1997
High School	Kenan Evren Lisesi	1991

FOREIGN LANGUAGES

Advanced English, Advanced Azerbaijani, Intermediate Russian

PUBLICATIONS

1. Evgeny Korelskiy, Tabiat Tan Yildiz, Jenis Urazaliev, Andrey Goloborodko, Artem Orlov, Suman Tirumanapalli, Roman Savinov, Marat Akhmetov, Ramon Ivanov, "Multidisciplinary engineering approach and proper planning enables successful drilling of one of the deepest exploration HPHT well in the Samgori-Patardzeuli, Georgia", SPE Russian Petroleum Technology Conference 2019, Moscow, Russia, SPE-196806, 22-24 October 2019
2. Tabiat Tan Yildiz, Rostislav Panferov, Yakov Shumakov, Dmitri Tsaplin, Jenis Urazaliev, Suman Tirumanapalli, Andrey Goloborodko, "Innovative and cost effective well testing solution for a tight oil and gas reservoirs",

AAPG GT, Exploration and Production in the Black Sea, Batumi, Georgia, 18-19 September 2019

3. Tabiat Tan Yildiz, Rosalind A. Archer, "Transient well index for numerical well test analysis", SPE Annual Technical Conference and Exhibition 2001, New Orleans, Louisiana, USA, SPE 71572, 30 September - 3 October 2001

WORK EXPERIENCE

Position	Organization	Year
Consultant	KOC - Kuwait Oil Company	2024 - Present
Field Development Director	Naphtho Energy - International Projects	2020 - 2024
Senior Reservoir Engineer	Schlumberger - Data and Consulting Services	2008 - 2020
Reservoir Engineer	TPAO - International Projects Group	2001 - 2008
Research Assistant	TAMU - Petroleum Engineering	1999 - 2001